ACS APPLIED BIO MATERIALS

www.acsabm.org Review

Giant Magnetoresistance Based Biosensors for Cancer Screening and Detection

Shahriar Mostufa, Bahareh Rezaei, Parsa Yari, Kanglin Xu, Jenifer Gómez-Pastora, Jiajia Sun, Zongqian Shi, and Kai Wu*

Cite This: *ACS Appl. Bio Mater.* 2023, 6, 4042−4059 Read Online

ACCESS | Metrics & More | Article Recommendations

ABSTRACT: Early-stage screening of cancer is critical in preventing its development and therefore can improve the prognosis of the disease. One accurate and effective method of cancer screening is using high sensitivity biosensors to detect optically, chemically, or magnetically labeled cancer biomarkers. Among a wide range of biosensors, giant magnetoresistance (GMR) based devices offer high sensitivity, low background noise, robustness, and low cost. With state-of-the-art micro- and nanofabrication techniques, tens to hundreds of independently working GMR biosensors can be integrated into fingernail-sized chips for the simultaneous detection of multiple cancer biomarkers (i.e., multiplexed assay). Meanwhile, the miniaturization of GMR chips makes them able to be integrated into point-of-care (POC) devices. In this review, we first introduce three types of GMR biosensors in terms of their structures and physics, followed by a discussion on fabrication techniques for those sensors. In order to achieve target cancer biomarker detection, the GMR biosensor surface needs to be subjected to biological decoration. Thus, commonly used methods for surface functionalization are also reviewed. The robustness of GMR-based biosensors in cancer detection has been demonstrated by multiple research groups worldwide and we review some representative examples. At the end of this review, the challenges and future development prospects of GMR biosensor platforms are commented on. With all their benefits and opportunities, it can be foreseen that GMR biosensor platforms will transition from a promising candidate to a robust product for cancer screening in the near future.

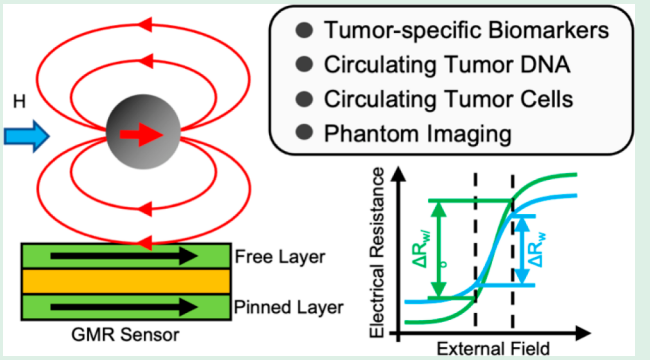

KEYWORDS: *giant magnetoresistance, biosensor, cancer screening, multiplexed assay, point-of-care*

1. INTRODUCTION

The current biosensors can be classified into two categories: label-based biosensors and label-free biosensors. Label-based biosensors involve the use of a labeled molecule, such as a fluorescent dye, enzyme, or nanoparticle, to detect and quantify the target analyte. These sensors provide a signal that can be measured or detected, indicating the presence or concentration of the analyte. Label-based platforms often provide enhanced sensitivity and signal amplification with the labeled molecules. Some common types of label-based biosensors include fluorescence-based biosensors,[1,2] enzyme-linked immunosorbent assays (ELISAs),[3,4] electrochemical biosensors with redox labels,[5−7] and magnetic biosensors with magnetic labels.[8,9] Label-free biosensors, on the other hand, do not require the use of a labeled molecule for detection. Instead, they directly measure the interaction between the target analyte and the sensor surface. Although label-free biosensors offer several advantages such as simplicity, real-time monitoring, and the ability to study biomolecular interactions without the need for labeling agents, they often lack signal amplification, resulting in lower sensitivity and detection limits. Some examples of label-free biosensors include surface plasmon resonance (SPR) biosensors,[10−12] quartz crystal microbalance (QCM) biosensors,[13] and interferometric biosensors.[14]

Among the label-based approaches, there are several types of biosensors that are widely used. Fluorescent biosensors are among the most employed, utilizing fluorescent labels that emit light of specific wavelengths upon excitation. They offer high sensitivity and are extensively utilized in molecular biology, medical diagnostics, and cellular imaging.[15−18] Enzymatic biosensors utilize enzymes as labels to catalyze specific reactions in the presence of the target analyte,

Received: July 28, 2023
Accepted: September 8, 2023
Published: September 19, 2023

https://doi.org/10.1021/acsabm.3c00592
ACS Appl. Bio Mater. 2023, 6, 4042−4059

generating detectable signals such as colorimetric or electrochemical changes.[19−21] These biosensors find applications in clinical diagnostics and environmental monitoring. On the other hand, magnetic biosensors offer several advantages in the field of bioanalysis.[22−26] First, biofluidic samples and biological tissues are para- or diamagnetic, exhibiting minimal interference with the generated magnetic signal, resulting in a low background noise during detection. Additionally, magnetic nanoparticle (MNP) and magnetic bead (MB) labels used in magnetic bioassays are generally cheaper and more stable under extreme biochemical conditions compared to other labeling techniques.[9,27] Furthermore, magnetic fields exhibit the ability to permeate biological tissues, enabling the remote modulation or control of magnetic bioassays. One practical application of this technology is magnetic separation, which can be employed for sample pretreatment to enrich the target analytes.[28−32] These advantages make magnetic biosensors a promising technology for various biomedical and clinical applications.

In this comprehensive review, we focus on the widely utilized giant magnetoresistance (GMR) based biosensors, renowned for their robustness and sensitivity.[33−35] These biosensors exploit the GMR effect, which refers to the change in electrical resistance R when a magnetic field is applied to a GMR device comprised of multiple magnetic layers separated by a nonmagnetic spacer (this applies to the most popular multilayer and spin valve GMR structures). The resistance change, ΔR, exhibits high sensitivity toward magnetic labels, enabling the detection and quantification of biological analytes. GMR-based biosensors have demonstrated reliable performance and have been extensively employed in diverse fields such as biotechnology, medical diagnostics, environmental monitoring, and more.[36−42] Their versatility and sensitivity make them valuable tools in various applications.

This review is divided into several sections to provide a comprehensive overview of GMR biosensor structures and their applications for cancer detection. In section 2, we present an overview of various types of GMR biosensor structures, including the multilayer, spin valve, and granular structures. We also discuss GMR biosensor patterns, surface chemical functionalization techniques, and GMR-based bioassay mechanisms. Blood-based biomarkers, such as genomic, transcriptomic, proteomic, and other cellular components, have shown great potential for minimally invasive cancer detection and assessment.[43−45] Thus, in section 3, we categorize different cancer detection works based on the type of the target analyte. Briefly, we cover protein biomarker detection, circulating tumor DNA (ctDNA) detection, direct tumor cell detection, and indirect tumor phantom detection. In the final part of this review, we evaluate the progress made in GMR-based biosensors for cancer screening and detection. We analyze the current advancements and identify the gaps in this field. Furthermore, we discuss the future development trends that can shape the future of GMR-based biosensors in cancer research and detection.

2. GIANT MAGNETORESISTANCE (GMR) BASED BIOSENSORS

2.1. Different Types of GMR Biosensors. The GMR effect is a quantum mechanical phenomenon first observed in metallic multilayer structures that are composed of alternating ferromagnetic (FM) and nonmagnetic (NM) conductive layers. GMR was independently reported by Albert Fert's and Peter Grünberg's teams in 1988.[46,47] Later, this discovery was recognized by the 2007 Nobel Prize in Physics. The GMR effect describes the change of electrical resistance in a GMR structure depending on the relative alignments of magnetizations in adjacent FM layers, due to spin-dependent scattering. In a magnetic system, the scattering of conduction electrons on the magnetic sublattice of the crystal affects the electrical resistance. Based on this, the GMR effect can be described by the famous two-current model.[48,49] When the magnetizations of neighboring FM layers are aligned parallel to each other, the scattering of conduction electrons is weak, resulting in low resistance. Conversely, when the magnetizations are antiparallel, the scattering is strong, leading to high resistance. The GMR effect has had significant implications in various technological applications, particularly in the field of magnetoresistive random-access memory (MRAM), where it has enabled the development of high-density, nonvolatile memory devices with improved performance and efficiency.[50−52]

There are three types of GMR structures that have been reported so far: GMR multilayer, spin valve (which also includes the pseudo spin valve), and granular GMR. The GMR multilayer structure is the most widely recognized and is shown in Figure 1A. The first GMR effect observed by Albert Fert's and Peter Grünberg's teams belongs to this type of structure. In a GMR multilayer structure composed of alternating FM and NM layers, the thickness of the NM layer is chosen such that the adjacent FM layers are antiferromagnetically coupled.[48] Thus, in the absence of external magnetic fields, the magnetizations in adjacent FM layers are aligned antiparallel. An external magnetic field could align the magnetizations parallel and, thereby, change the electrical resistance of the structure. The overall electrical resistance of this structure is relatively low for parallel alignment and relatively high for antiparallel alignment.

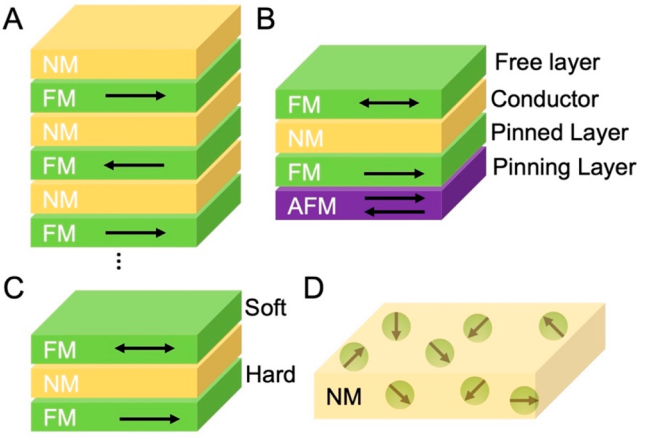

Figure 1. Schematic views of (A) GMR multilayer structure, (B) spin valve structure, (C) pseudo spin valve structure, and (D) granular GMR structure.

In a GMR spin valve structure, as shown in Figure 1B, the GMR effect comes from the exchange bias, where the magnetization in one of the FM layers is exchange biased (or "pinned") by the adjacent antiferromagnetic (AFM) layer while the magnetization in the other FM layer is "free" to switch. Thus, the magnetizations in the "free layer" and "pinned layer" switch at different values of the magnetic fields.

https://doi.org/10.1021/acsabm.3c00592
ACS Appl. Bio Mater. 2023, 6, 4042−4059

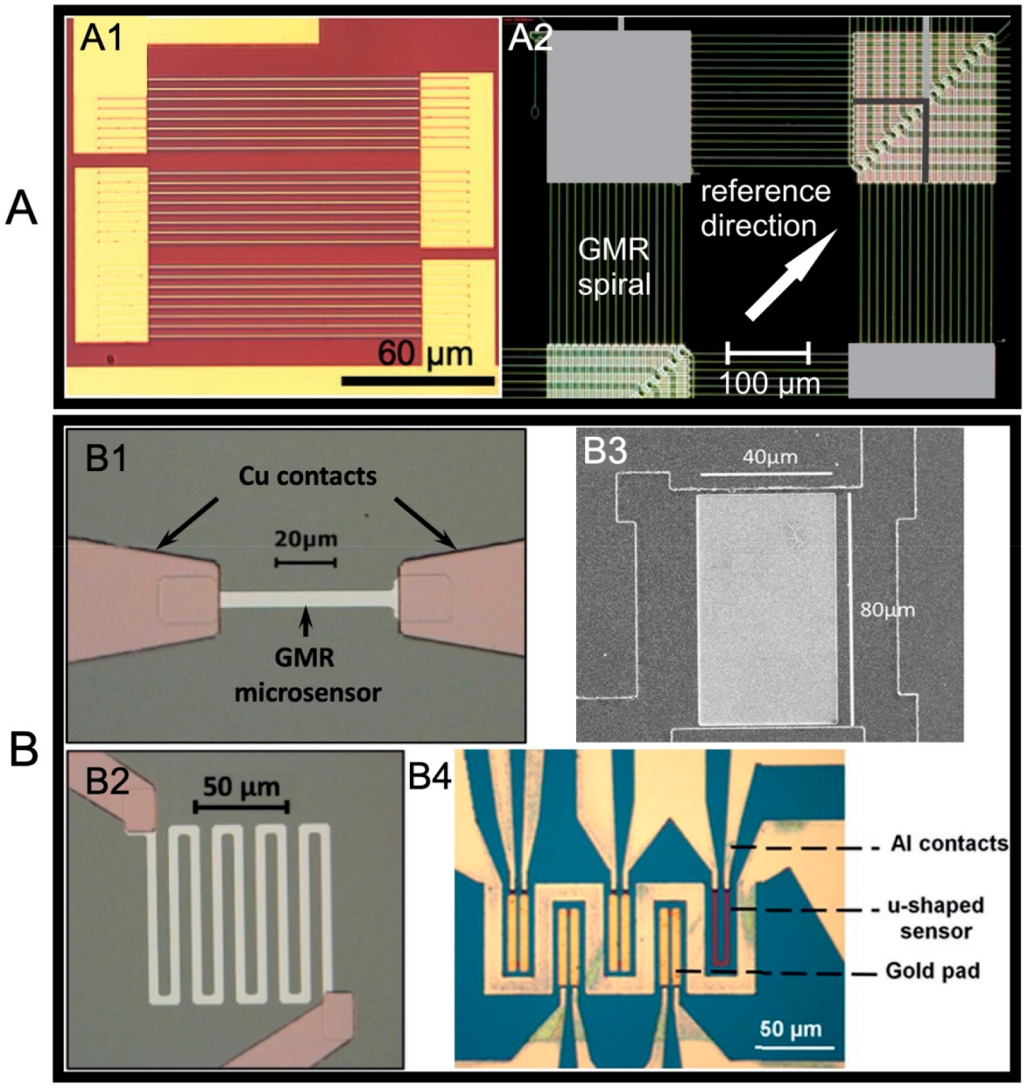

Figure 2. Different GMR biosensor patterns. (A) Thin stripe GMR biosensors. (A1) Each GMR thin stripe has an area of 150 μm × 0.75 μm. (A2) Each GMR spiral shape sensor has a width of 160 nm. (B) Large area GMR biosensors. (B1) Each GMR thick stripe biosensor and (B2) each GMR meander shape biosensor has a width of 6 μm. (B3) Each GMR rectangular shape biosensor has an area of 80 μm × 40 μm. (B4) Each leg of the "U" shape GMR biosensor has an area of 2.5 μm × 80 μm. (A1) From ref 57. CC BY 4.0. (A2) Reproduced with permission from ref 58. Copyright 2012 American Institute of Physics. (B1, B2) From ref 59. CC BY NC 4.0. (B3) Reproduced with permission from ref 55. Copyright 2017 American Institute of Physics. (B4) Reproduced with permission from ref 60. Copyright 2016 The Royal Society of Chemistry.

This type of GMR responses to external magnetic fields by changing the magnetization orientation in the "free layer" relative to the "pinned layer". On a separate note, the pseudo spin valve structure has also been reported; see Figure 1C, where the AFM layer is missing. The two FM layers in a pseudo spin valve are made of different materials and show different magnetic coercivities. One FM layer has low coercivity and is called the soft FM layer (acting like the "free layer" in the spin valve), and the other (with high coercivity) is called the hard FM layer (like the "pinned layer" in the spin valve). This difference allows the two FM layers to switch at different values of magnetic fields.

Granular GMR structures are composed of FM particles, or grains, embedded within an NM conductive layer. The working principle of granular GMR is based on the spin-dependent scattering of electrons at the surface and in the bulk of these FM particles. The structure of a granular GMR device is depicted in Figure 1D. The FM particles, which have inherent magnetic properties, are distributed throughout the NM conductive layer. This arrangement allows for interactions between the electrons in the NM layer and the magnetizations of the FM particles. When an electric current flows through the granular GMR structure, electrons move through the NM layer and encounter the FM grains. The scattering of electrons occurs at the surface and within the grains. The scattering processes are spin dependent. The resistance of the granular GMR structure is also sensitive to the magnetic field applied to it. When an external magnetic field is present, it can alter the orientation of the magnetic moments in the FM grains. As a result, the scattering behavior of the electrons changes, affecting the overall resistance of the device.

Among all the GMR structures reviewed in this section, the spin valve GMR biosensors have emerged as the preferred choice for biosensing applications, surpassing GMR multilayer and granular GMR sensors due to several distinct advantages. First, spin valves exhibit heightened sensitivity, particularly in

https://doi.org/10.1021/acsabm.3c00592
ACS Appl. Bio Mater. 2023, 6, 4042−4059

small fields. This increased sensitivity enables the detection of minute changes in the magnetoresistance signal, facilitating the identification of lower concentrations of target analytes in biosensing applications. Second, they offer a superior signal-to-noise ratio, effectively distinguishing the signal of the target analyte from the background noise. Consequently, these biosensors provide enhanced accuracy and reliability in biosensing measurements. Third, they offer improved long-term stability, as they are less susceptible to drift and environmental changes. This ensures consistent and reliable performance over extended periods of time. Moreover, spin valves can be easily fabricated using standard semiconductor manufacturing processes, thanks to their simple stack structures. This ease of fabrication has expanded their potential applications in various fields, including medical diagnostics, environmental monitoring, and food safety, where the precise and sensitive detection of biomolecules is vital. Notably, to the best knowledge of the authors, all the reviewed works on GMR-based cancer detection and screening presented in this publication are based on GMR spin valve biosensors.

2.2. Different GMR Biosensor Patterns. With the advancements in micro- and nanofabrication techniques, individually operating GMR biosensors typically range in size from tens to hundreds of micrometers. Figure 2 demonstrates the potential scalability of GMR biosensors, with the theoretical possibility of over 1 million sensors per square centimeter.[35,53] To date, various GMR biosensor patterns have been reported, primarily distinguished by the width of the GMR biosensors. These patterns can be broadly classified into two types: (1) thin stripes with widths below 1 μm, such as the thin stripe and spiral shapes depicted in Figure 2A1,A2; (2) large area patterns with widths exceeding 1 μm, such as the thick stripe, meander, rectangular, and "U" shapes shown in Figure 2B1−B4. Notably, in GMR-based bioassays, it has been observed that the placement of magnetic labels at the sensor edges generates greater GMR signal variations (such as the resistance R and magnetoresistance MR) compared to when the labels are situated directly in the center of the sensor surface.[54] This finding encourages the design of GMR biosensors with higher aspect ratios, such as thin stripes and spiral shapes. Conversely, large area GMR biosensors enable the detection of magnetic labels through a local magnetic reversal nucleation mechanism.[55,56] As a result, the authors of this work have classified GMR biosensors based on their width, taking into account the various mechanisms that cause the GMR signal change.

In addition to considering the sensor pattern design driven by the sensing mechanism, practical factors need to be considered when designing GMR biosensors. Sensors with high aspect ratios, such as the thin stripes illustrated in Figure 2A, pose a higher risk of open circuitry. Even minor defects in the GMR thin films/substrates can lead to breakage in these GMR biosensors. To address this issue, connecting multiple GMR thin stripes in series and in parallel can provide a solution. For instance, in Figure 2A1, one GMR biosensor comprises three groups of GMR thin stripes connected in series, with each group containing eight GMR stripes connected in parallel. By connecting the GMR stripes in series, the risk of open circuitry can be minimized, while connecting them in parallel serves to increase the overall resistance and improve the signal-to-noise ratio.

Another challenge faced by thin stripe GMR biosensors is their limited effective sensing area. In comparison to large area GMR biosensors, the effective sensing area of thin stripe GMR biosensors is reduced due to the presence of spacers between sensor stripes (as depicted in Figure 2A1). Consequently, some magnetically labeled target analytes may land on these spacers, failing to contribute to the GMR signal. Additionally, bioassay repeatability becomes a concern, especially when measuring low abundance target analytes. This is because the captured MNP labels are randomly distributed across both the sensor regions and spacer areas. To tackle these challenges, certain research groups tend to favor the utilization of large area GMR biosensors.

2.3. GMR Biosensor Surface Chemical Functionalization. In the last step of fabricating GMR biosensors, the sensor surface is usually deposited with a thin layer of insulator such as SiO_2, Al_2O_3, Si_3N_4, etc.[61−63] There are three major functions of this insulating layer:

(1) Isolate GMR thin films from the external biological environment. Since the magnetic materials in the GMR thin films are cytotoxic and the biological fluids are corrosive to GMR biosensors, this insulating layer can effectively protect the GMR biosensors from directly interfacing with the external environment.
(2) Prevent leakage current from GMR biosensors to the biological sample.
(3) Furnish chemical groups that aid in the subsequent step of surface chemical modification.

Since the magnetic signal (i.e., the dipolar magnetic field) from the magnetic labels drops off with the cube of the distance, this insulating layer inevitably increases the distance from magnetic labels to GMR biosensors. Thus, there is a trade-off in the thickness of this insulating layer; namely, it should be thick enough to effectively isolate the GMR biosensors from the external environment but at the same time it should be thin enough to avoid degrading the detection capacity of GMR biosensors. Typically, this layer is reported to be in the range of tens to hundreds of nanometers thick.[64,65]

To functionalize GMR biosensors for the specific detection of cancer biomarkers as well as cancer cells, the GMR biosensor surface needs to be activated to allow the effective coupling of capture probes (including capture antibodies, capture DNA probes, etc.). There are two popular methods to achieve this surface modification, namely, 3-aminopropyltriethoxysilane/glutaraldehyde (APTES/GA)[65,66] and 1-ethyl-3-(3-(dimethylamino)propyl) carbodiimide/N-hydroxysuccinimide (EDC/NHS).[62,67,68] Herein, we briefly describe the steps to carry out the APTES/GA method to functionalize GMR biosensors with capture probes, as schematically drawn in Figure 3:

(1) Begin by sequentially washing the GMR biosensor chip with acetone, methanol, isopropanol, and deionized water to eliminate surface contaminants. Afterward, expose the GMR biosensor surface to oxygen plasma (e.g., for 3 min) to enhance the presence of hydroxyl groups on the insulating layer, thereby facilitating the surface functionalization process.
(2) Submerge the chip in a 0.5−1% APTES in toluene mixture (e.g., for 15 min), followed by rinsing with acetone and deionized water.
(3) Immerse the chip in a 5.0% GA in water solution (e.g., for 5 h), then rinse with deionized water.
(4) Dispense capture probes on the GMR biosensors and incubate them at high humidity for 4 h to enable the

https://doi.org/10.1021/acsabm.3c00592
ACS Appl. Bio Mater. 2023, 6, 4042−4059

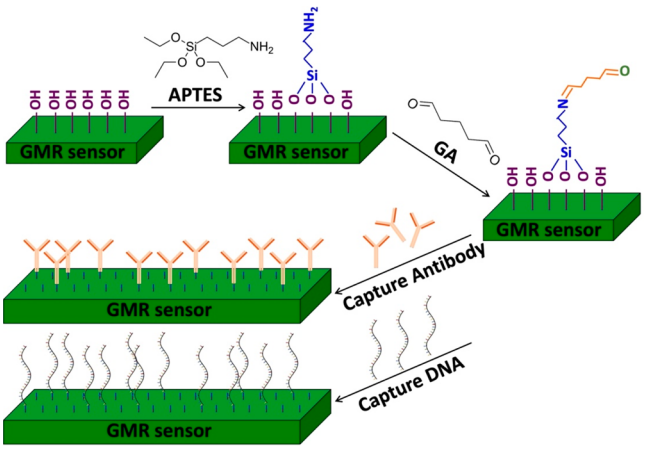

Figure 3. Schematic view of GMR biosensor surface functionalization with capture probes based on the APTES/GA method. Adapted from ref 69. CC BY 4.0.

effective immobilization of capture probes. Subsequently, rinse the biosensors with phosphate-buffered saline (PBS) to remove any unbound capture probes.

Specifically, after the initial pretreatment step, the GMR biosensor surfaces exhibit increased hydrophilicity, making them more amenable to subsequent chemical treatments and protein grafting. Figure 3 illustrates the APTES/GA modification method, wherein the GMR biosensor surface undergoes treatment with APTES. The silanol groups within APTES attach to the hydroxyl groups (−OH) present on the surface of the insulating layer, initiating internal polymerization of silanes to form Si−O−Si (siloxane) linkages. Consequently, amine groups ($-NH_2$) become exposed at the opposite end of the siloxane bonds. Subsequently, the GA solution is introduced, wherein one of the two aldehyde groups (−CHO) covalently binds to the amine group originating from APTES. The remaining reactive aldehyde group forms a covalent bond with the amine groups of the capture probes. The capture antibodies and capture DNA with one end attached to the amine groups are depicted in Figure 3.

Alternative surface modification techniques have also been documented, such as those utilizing polyvinyl chloride (PVC),[63] polyethylenimine (PEI),[70] and epoxysilane (3-glycidoxypropyl-trimethoxysilane),[71] among others. After the functional group modification but before immobilization of the capture probes, GMR biosensors/chips can be stored in a dry environment until the capture probes are attached.

It is worth mentioning that, after the immobilization of capture probes, the GMR biosensors should be treated with 1−10% bovine serum albumin (BSA) in PBS buffer for 1 h to block the remaining binding sites from the biosensor surface (i.e., the remaining reactive aldehyde groups). This step can effectively reduce the nonspecific binding during the bioassay process, thus lowering the false positive (FP) rate. Then, the GMR biosensor should be stored at 2−8 °C in a humid environment until use. The empirical shelf life of capture antibody functionalized GMR chips is 2 weeks until the capture antibodies get inactivated. Note that the performance of GMR biosensors is stable over time. One solution to extend

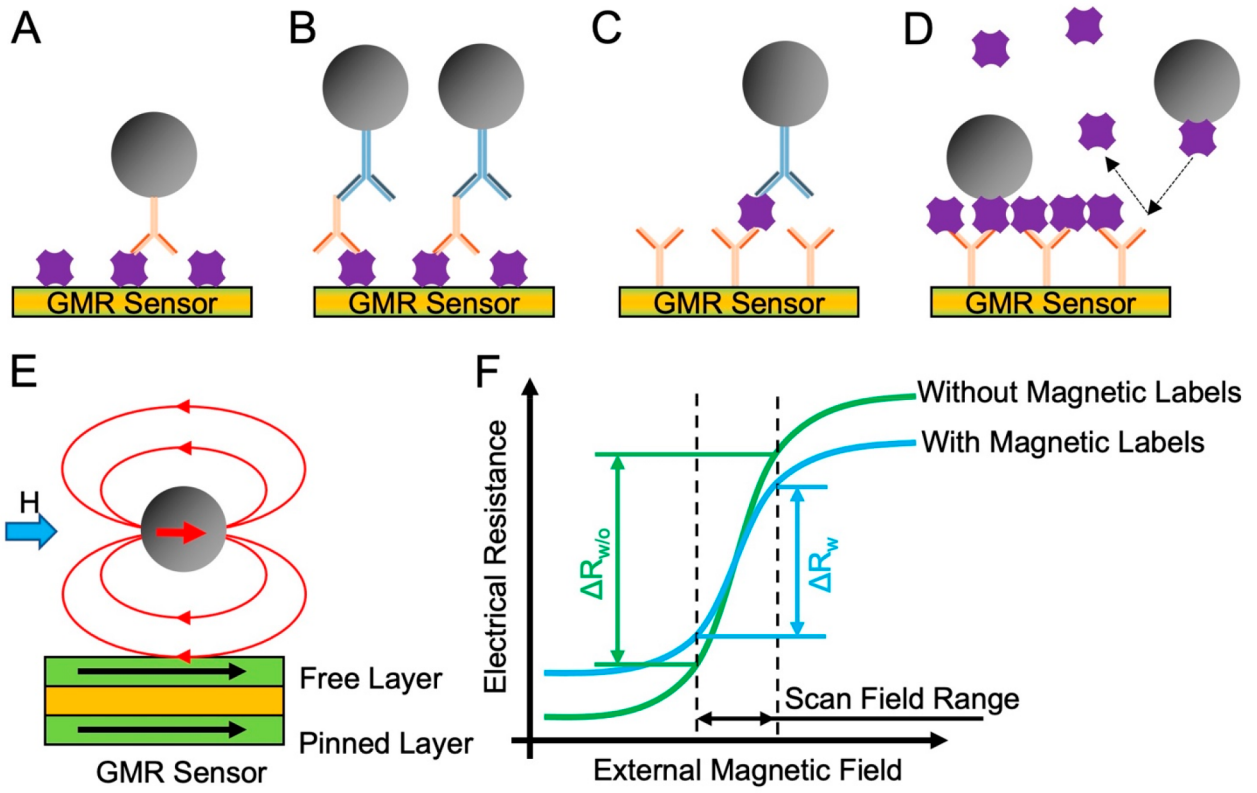

Figure 4. Schematic view of GMR-based bioassay mechanisms: (A) direct assay; (B) indirect assay; (C) sandwich assay; (D) competitive assay. (E) GMR biosensor for detecting magnetically labeled target analytes. (F) RH transfer curve of a GMR biosensor before and after capturing magnetic labels.

https://doi.org/10.1021/acsabm.3c00592
ACS Appl. Bio Mater. 2023, 6, 4042−4059

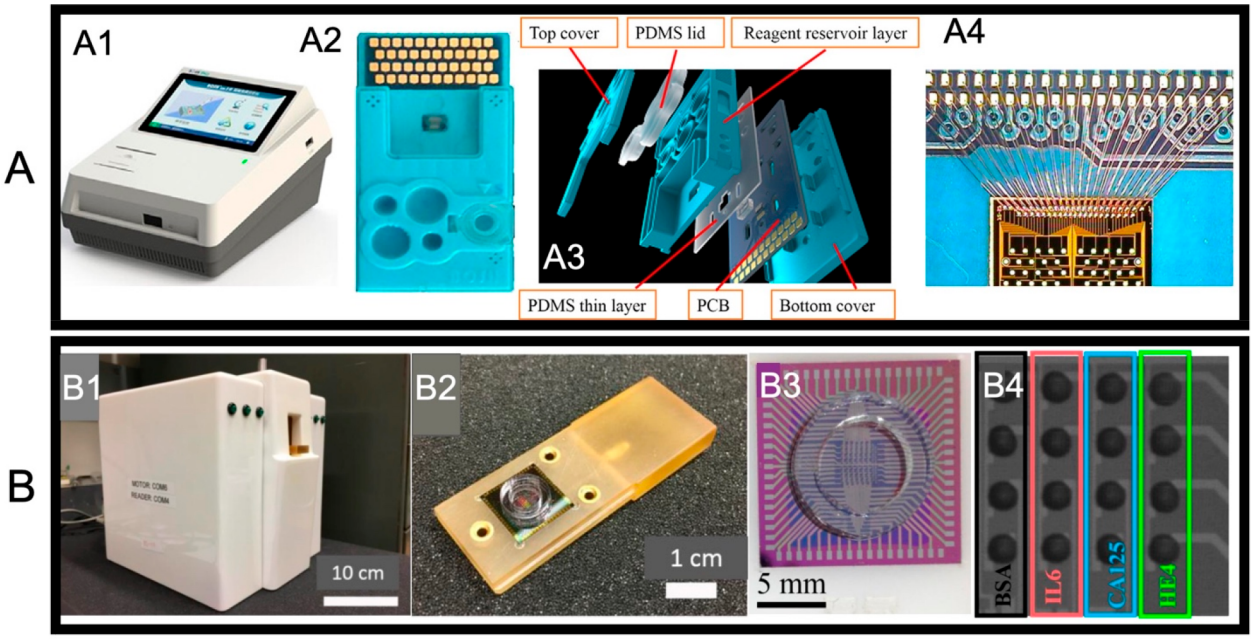

Figure 5. (A) GMR POCT for the detection of 12 tumor biomarkers. (A1) Photograph of the GMR POCT reported by Gao et al.[63] (A2) Photograph of the test card. (A3) Schematic view of the multilayer structure of the test card. (A4) Photograph of one GMR biosensing chip and its connection with the PCB. (B) GMR benchtop system for the detection of three ovarian cancer biomarkers reported by Klein et al.[77] (B1) Photograph of the benchtop GMR base station, with an overall size of 20 cm × 20 cm × 20 cm. (B2) Photograph of the GMR chip holder, namely, the cartridge. (B3) Photograph of one disposable GMR biosensing chip. (B4) Photomicrograph of the GMR biosensor array after dispensing with CA125 II capture antibody, HE4 capture antibody, IL6 capture antibody, and BSA each column. Each GMR sensor was completely covered with 1.2 nL of capture antibodies (500 μg/mL) or BSA (10 mg/mL). (A) Reproduced with permission from ref 63. Copyright 2018 Elsevier B.V. (B) Reproduced with permission from ref 77. Copyright 2018 Elsevier B.V.

the shelf life of functionalized GMR chips is to lyophilize the capture probes.

2.4. GMR-Based Bioassay Mechanisms. Bioassays are carried out on functionalized GMR biosensors to quantify the target biomarkers, chemicals of biological interest, or target cells. In this context, we will discuss the bioassay mechanism using the antibody-based immunoassay as an example. Based on the characteristics of target protein analytes (molecular weight, concentration, etc.) and different requirements for carrying out the analysis, there are four types of GMR-based bioassay mechanisms as shown in Figure 4A–D: (1) direct assay, (2) indirect assay, (3) sandwich assay, and (4) competitive assay.

In a direct assay (see Figure 4A), the GMR biosensor surface is functionalized with target analytes (e.g., antigen), and then the magnetically labeled antibodies are added and incubated to allow the specific antibody–antigen bonding. The unbound antibody–magnetic label complexes are removed by a wash step.

In an indirect assay (see Figure 4B), the GMR biosensor surface captures the target analyte (e.g., primary antibody) via the antigen. Subsequently, magnetically labeled secondary antibodies are introduced, specifically binding to the primary antibody, thus completing the detection process.

The most popular and robust bioassay method is the sandwich assay, shown in Figure 4C, where the capture antibodies are functionalized on the GMR biosensor surface and then the biofluidic sample containing target analytes is added to specifically bind the target analytes to these capture antibodies. After a wash step, the magnetically labeled detection antibodies are added to specifically bind to target analytes and form a "sandwich" structure. Due to its intrinsic high detection specificity (two antibodies are used for capture and detection processes), this sandwich bioassay method is the most frequently used and reported in the literature.

In a competitive assay (Figure 4D), a limited number of antibodies are functionalized on the GMR biosensor surface. Then, the free target analytes from the biological sample will compete for the limited antibody binding sites with the magnetically labeled analytes. Thus, biological samples containing a higher amount of free target analytes result in more unlabeled analytes occupying the binding sites. Vice versa, biological samples containing lower amounts of free target analytes lead to more magnetically labeled analytes captured onto the sensor surface. Competitive assays are often used to detect small biomolecules with molecular weights smaller than 10 000 Da.[72] Typically, for small biomolecules of this type, there is insufficient space to accommodate more than one epitope for antibody binding.

For all kinds of bioassay mechanisms, the ultimate result is the capture of magnetic labels on the GMR biosensor surface due to specific binding. Upon the application of an external magnetic field (also called scan field), as shown in Figure 4E, these captured magnetic labels are magnetized and generate dipolar fields that alter the local magnetization in the "free layer" of a GMR spin valve. As a result, the shape of the *RH* (resistance–field) transfer curve changes (see Figure 4F). Within a scanning field range, the change of the electrical resistance ΔR ($=R_{high} - R_{low}$), or voltage ΔV, or magnetoresistance ratio (MR, $\Delta R/R_{high/low} \times 100\%$) can be used for quantitative detection of target analytes. It should be noted that the *RH* curves depicted in Figure 4F have been simplified and exaggerated to illustrate the impact of magnetic labels on

https://doi.org/10.1021/acsabm.3c00592
ACS Appl. Bio Mater. 2023, 6, 4042–4059

the GMR biosensor's surface, influencing the electrical resistance.

3. GMR BIOSENSORS FOR CANCER SCREENING AND DETECTION

3.1. GMR Biosensors for Tumor-Specific Protein Biomarker Detection. Cancer detection and screening based on tumor-specific protein biomarkers have garnered significant attention in the field of oncology.[73−76] Biomarkers are specific molecules that can indicate the presence of cancer or provide insights into disease progression and response to treatment. Tumor-specific protein biomarkers, such as certain antigens or enzymes, are produced or overexpressed by cancer cells, making them valuable indicators for early detection and monitoring of cancer-related conditions. Utilizing immunoassays and molecular diagnostics, researchers and clinicians have made significant strides in detecting these biomarkers with high sensitivity and specificity. Early detection of cancer through the identification of tumor-specific protein biomarkers allows for timely intervention, facilitating treatment initiation at earlier stages when outcomes are generally more favorable. Moreover, these biomarkers play a crucial role in developing personalized treatment plans, enabling healthcare professionals to tailor therapies based on individual patients' specific cancer profiles. Overall, the detection and screening of cancer using tumor-specific protein biomarkers hold great promise in improving patient survival rates and enhancing the overall effectiveness of cancer management strategies. In this section, we review some examples of applying GMR biosensors for tumor-specific protein biomarker detection.

Gao et al. conducted a comprehensive study and devised a GMR-based multibiomarker point-of-care testing (POCT) diagnostic system,[63] presented in Figure 5A1. This system exhibits the capability to simultaneously detect 12 distinct tumor markers through the integration of a GMR sensor chip, a microfluidic channel, MNP labels, and a double antibody sandwich immunization mechanism. The investigated biomarkers encompass a range of tumor-related proteins, namely, α-fetoprotein (AFP, 70 kDa), carcinoembryonic antigen (CEA, 180 kDa), cytokeratin 19 fragment (CYFRA21-1, 40 kDa), neuron-specific enolase (NSE, 47 kDa), free β-subunit of human chorionic gonadotropin (free-β-hCG, 23.5 kDa), squamous cell carcinoma antigen (SCC, 45 kDa), pepsinogen I (PG I, 42 kDa), pepsinogen II (PG II, 42 kDa), total prostate-specific antigen (total PSA, tPSA, including PSA-ACT (90 kDa) and free PSA), free prostate-specific antigen (free PSA, fPSA, 34 kDa), thyroglobulin (Tg, 660 kDa), and carbohydrate antigen 19-9 (CA19-9, >400 kDa). Figure 5A2,A3) showcases an all-in-one test card with a comprehensive six-layer configuration. The layers include a top cover, a polydimethylsiloxane (PDMS) lid, a reagent reservoir layer, a PDMS thin layer, a printed circuit board (PCB) housing the GMR chip, and a bottom layer. The reagent reservoir layer contains specialized cavities for housing the sample, washing solution, and MNP solution. To secure the reagent reservoir cavities, the PDMS lid is firmly attached, providing an effective seal. A microfluidic channel, located beneath the reagent reservoir layer, connects the reservoir to the reaction chamber situated above the GMR biosensing chip. This microfluidic channel is sealed using a PDMS thin film. The microfluidic control system operates in a pressure-driven flow mode, allowing for fully automatic bioassays with multiple wash steps to efficiently remove any unbound reagents. This well-designed system enables streamlined and reliable detection of target biomolecules, enhancing the overall efficiency and accuracy of the bioassay process.

For this device, the GMR spin valve biosensors on the GMR chip are composed of a stacked structure consisting of PtMn (10 nm)/CoFe (2 nm)/Cu (1.2 nm)/CoFe (1 nm)/NiFe (3 nm)/Al_2O_3 (40 nm), where the PtMn serves as the AFM layer to "pin" the neighboring CoFe FM layer. CoFe (1 nm)/NiFe (3 nm) is the composite FM "free" layer to sense the MNP labels that are captured on the sensor surface. In Figure 5A4), it can be observed that the GMR chip contains 40 individual GMR biosensors, each with a diameter of 120 μm. Each sensor is designed to detect a specific type of tumor-specific protein, enabling the simultaneous detection of up to 40 different proteins. This multianalyte assay offers substantial benefits compared to single-analyte tests, including cost efficiency, reduced labor, and enhanced convenience. By enabling simultaneous measurement of multiple biomarkers in serum samples with exceptional sensitivity and accuracy, this immune sensor holds promise for early tumor diagnosis. The authors[63] assessed the robustness of their GMR biosensor platform by conducting a comparative analysis with established Architect assays (for SCC, PG I, PG II) and Roche assays (for CEA, AFP, total PSA, free PSA, CYFRA21-1, NSE, free-β-hCG, Tg, CA19-9) using clinical samples. The results revealed that their GMR biosensors exhibited strong correlation coefficients (R^2 > 95%) and slopes (close to 1) when detecting 12 tumor markers (details not presented here).

In a different work, Xu et al. presented a GMR chip for the detection of four prostate cancer related autoantibodies—Parkinson disease 7 (PARK7), the TAR DNA-binding protein 43 (TARDBP), Talin 1 (TLN1), and Caldesmon 1 (CALD1)—as well as the PSA protein and the free/total PSA ratio.[78] Their study aimed to differentiate prostate cancer from noncancer cases using human serum samples from 99 patients, consisting of 50 noncancer cases and 49 clinically localized prostate cancer cases. To detect prostate cancer related autoantibodies, an indirect assay mechanism was employed, involving the immobilization of multiple recombinant proteins on distinct GMR biosensor surfaces. Following a wash step, serum samples at a 1:100 dilution were applied to the sensors, allowing target autoantibodies in the serum to bind to the capture proteins, subsequently conjugated with antihuman IgG antibodies (biotinylated) that were labeled with MNPs. On the other hand, for free and total PSA detection, a sandwich assay was conducted. The GMR biosensing system utilized a chip with 72 effective sensors and 8 reference sensors, measuring 10 × 12 mm. This chip featured a central array of 10 × 8 sensors with a spacing of 400 μm between adjacent sensors. The assay demonstrated exceptional performance without cross-reactivity, and all autoantibody assays exhibited statistically significant differences between prostate cancer and noncancer samples, except for PARK7. Notably, the combination of the four autoantibodies as a panel, along with the free/total PSA ratio, yielded the most significant difference, achieving the highest area under the curve (AUC) of 0.916 in receiver operating characteristic (ROC) analysis.

In another example, Klein et al. reported a benchtop and hand-held GMR bioassay platform and applied it for the detection of ovarian cancer.[77] This portable prototype system demonstrated high-sensitivity multiplex assays adaptable for various diseases, including ovarian cancer. It successfully

https://doi.org/10.1021/acsabm.3c00592
ACS Appl. Bio Mater. 2023, 6, 4042−4059

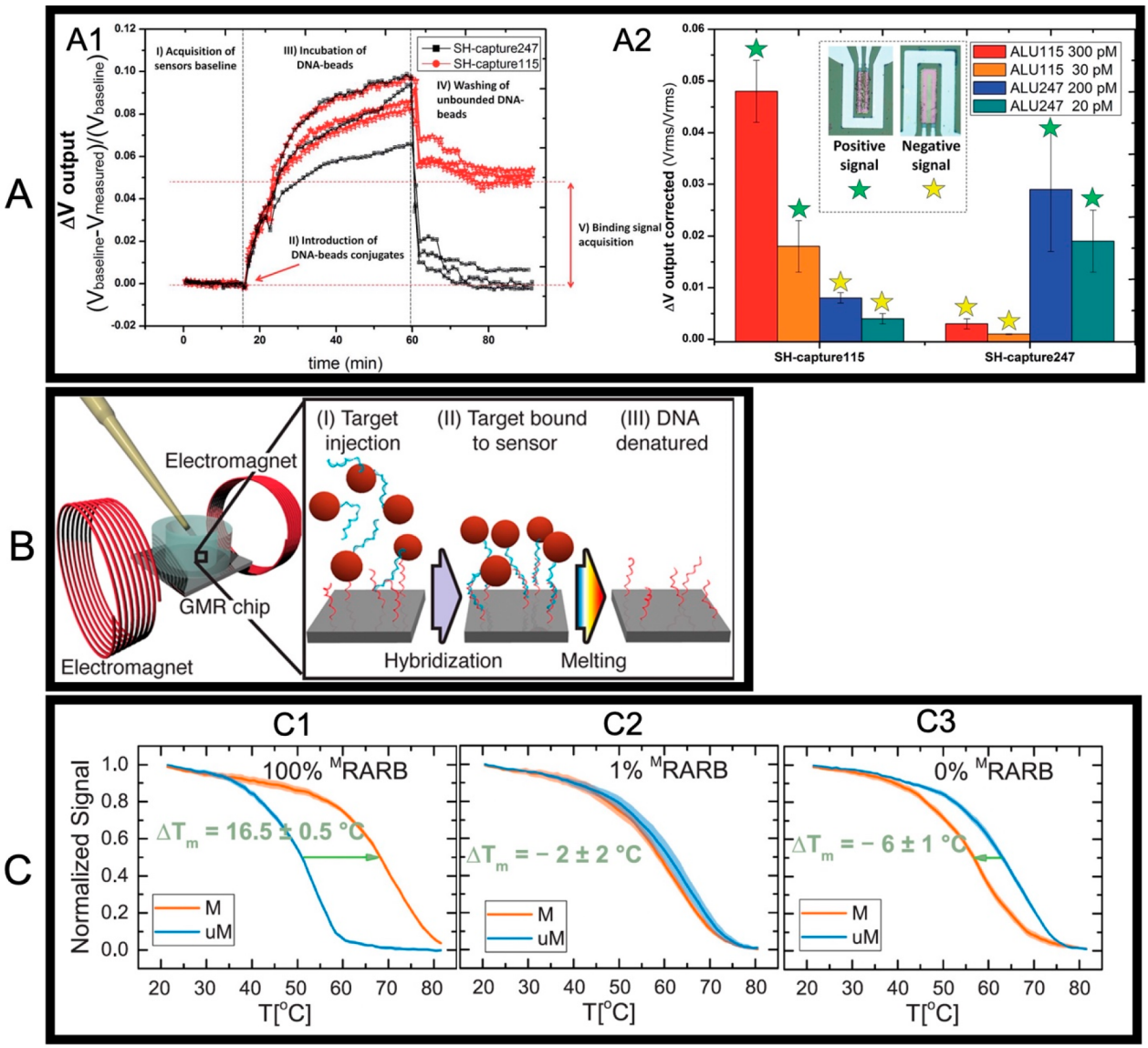

Figure 6. (A) GMR biosensor for the detection of ALU115 and ALU247. (A1) Signal response for the detection of ALU115 (300 pM) by GMR biosensors functionalized with complementary SH-probe115 (red curves) and biosensors functionalized with noncomplementary SH-probe247 (black curves). (A2) On-chip detection of ALU115 and ALU247. Data was obtained from the average of different GMR biosensors for each of the measurements (minimum = 8 sensors; maximum = 12 sensors). Error bars stand for standard error. (B) Schematic protocol for the detection of magnetically labeled DNA using GMR biosensors: (I) Denatured and labeled PCR products are injected onto the GMR chip, where they hybridize with surface-tethered probes at 37 °C for 1 h. (II) Unbound DNA is washed away, leaving the hybridized DNA on the sensor surface. (III) The temperature is gradually increased from 20 to 65 °C to measure the melting temperature, T_m. (C) GMR for multiplexed RARB/KIT methylation detection. (C1−C3) DNA melting curves measured on GMR sensors for (C1) 100, (C2) 1, and (C3) 0% ^{M}RARβ. ΔT_m is defined as the difference between the melting curve of the DNA hybridized to the M and uM capture probes. (A) Reproduced with permission from ref 60. Copyright 2016 The Royal Society of Chemistry. (B) Reproduced from ref 67. Copyright 2017 American Chemical Society. (C) Reproduced with permission from ref 97. Copyright 2018 Elsevier B.V.

detected cancer antigen 125 (CA125 II), human epididymis protein 4 (HE4), and interleukin 6 (IL6), with impressive limits of detection (LODs) as low as 3.7 U/mL, 7.4 pg/mL, and 7.4 pg/mL, respectively. Figure 5B1 showcases the utilization of the benchtop GMR base station to collect signals from a multiplex ovarian cancer assay. The fabricated GMR chips had dimensions of 15 mm × 15 mm (refer to Figure 5B3) and featured a single reaction well, enabling a one-time-use multiplexed immunoassay. Within each reaction well, four groups of GMR sensor arrays were organized in a 4 × 4 configuration. For this study, a specific group was selected (see Figure 5B4), while the other sensor groups were unused. Each GMR biosensor in the chosen group had an overall sensing area of 100 μm × 150 μm. These GMR biosensors consisted of five groups of GMR thin stripes connected in series, with a separation pitch of 3 μm. Additionally, each group contained 10 GMR thin stripes of 750 nm width connected in parallel. For the bioassay, the GMR chip was inserted into the benchtop GMR base station using a cartridge (see photograph in Figure 5B2), and a volume of 30 μL of PBS was added to the reaction well. After a 10 min warm-up period, a baseline was established for 3 min before the MNP labels were introduced. It is worth mentioning that a hand-held version, not depicted here, was also integrated with an identical circuit board.[65,66,79]

https://doi.org/10.1021/acsabm.3c00592
ACS Appl. Bio Mater. 2023, 6, 4042−4059

3.2. GMR Biosensors for Circulating Tumor DNA (ctDNA) Detection. The evaluation of circulating cell-free DNA (cfDNA) has emerged as a promising noninvasive method for cancer diagnostics.[80−83] The cfDNA primarily originates from dying cells through apoptosis or necrosis, a process extensively documented elsewhere. Acting as a liquid biopsy, cfDNA allows for the potential genotyping of somatic mutations originating from an individual's tumor site without the need for invasive biopsies. However, detecting cfDNA derived from tumors poses significant challenges due to the low abundance of circulating tumor DNA (ctDNA), which often represents less than 1.0% of the total cfDNA fraction. This limitation poses a challenge for most standard sequencing approaches. Various technologies are commonly used for ctDNA genomic profiling in clinical settings. These include amplification-refractory mutation system (ARMS) polymerase chain reaction (PCR) or ARMS-PCR assays,[84,85] pyrophosphorolysis-activated polymerization (PAP) assays,[86,87] digital methods such as beads, emulsion, amplification, and magnetics (BEAMing),[88] droplet digital PCR (ddPCR),[89,90] and next-generation sequencing (NGS) assays.[91,92] However, fluorescent assays typically exhibit lower analytical and clinical sensitivities, ranging from 75 to 100 copies/mL and 70% sensitivity, respectively.[93] Digital PCR has proven to be more sensitive than ARMS-PCR assays; however, its multiplexing capability is limited, and it requires specialized equipment to partition samples into individual droplets.[94] Conversely, NGS assays provide high sensitivity (detecting mutant allelic fractions as low as 0.1−0.01%) and multiplexing ability.[95] Nevertheless, NGS assays are often expensive and demand advanced technical skills and instrumentation that may not be readily available in clinical settings. Consequently, samples are frequently sent to centralized facilities for processing, resulting in potential delays of 2 weeks or more to obtain results. The integration of multiple functionalities in lab-on-a-chip devices offers significant advantages, including automation, cost-effectiveness, and speed. In this context, GMR-based biosensors have been reported for detecting biologically significant DNA fragments derived from blood samples. Leveraging the benefits of GMR technology, these biosensors present a promising approach for enhancing the efficiency and accessibility of molecular diagnostic assays in clinical applications.

In healthy individuals, apoptosis releases small DNA fragments (180−200 bp) into the bloodstream. In cancer patients, increased necrosis leads to higher levels of undigested DNA. Umetani et al. developed a method using quantitative real-time PCR (qPCR) to measure DNA integrity by assessing the ratio of longer to shorter fragments (ALU115 and ALU247).[96] This method has been applied for diagnosing gliomas and lobular breast cancer and detecting colorectal cancer stages. Later, in 2016, Dias et al. reported the detection of ALU115 and ALU247 with an integrated system based on a GMR sensor.[60] In their work, isolated cfDNA from blood samples was utilized, and qPCR was conducted for the amplification of ALU115 and ALU247. Two sets of primers were developed, with the sequences adapted from Umetani's work.[96] For ease of magnetic labeling, the primers were modified with a 5′-phosphorylated terminal group in the forward primers and a biotin moiety at the 5′-end of the reverse primers. The amplicons were then subjected to digestion by Lambda exonuclease, resulting in single-stranded products. To label the PCR products, 250 nm streptavidin coated magnetic beads (product code 09-19-252, Micromod) were employed. Single-stranded DNA (ssDNA) capture probes, SH-capture115 and SH-capture247, were thiolated at the terminus and functionalized on the GMR biosensor surface. It is important to note that their GMR biosensor surface was initially coated with a 300 nm thick SiN insulating layer, followed by a thin layer of Ti (5 nm)/Au (40 nm). The thiol−gold biochemistry enabled the immobilization of the ssDNA capture probes. Before conducting the bioassays, the researchers validated the efficiency of the cfDNA isolation and the generation of biotinylated ssDNA targets. They also optimized the hybridization process between the capture probes and target ssDNA. The detection of both targets was successfully validated in the picomolar range using an array of GMR biosensors, as illustrated in Figure 6A.

In Figure 6A1, the detection of magnetically labeled ALU115 at a concentration of 300 pM is illustrated. The measured signals underwent several phases: baseline acquisition ($V_{baseline}$), injection of magnetically labeled ssDNA targets onto the GMR biosensor surface, incubation to allow interaction between ssDNA targets and capture probes, washing to remove unbound magnetic beads, and acquisition of the binding signal ($V_{binding}$). The binding signal was subtracted from the baseline signal to obtain the output signal variation (ΔV_{output}). For signal normalization and correction, ΔV_{output} from each sensor was further adjusted by subtracting the output signal from reference sensors to account for thermal drifts. The resulting signal, $\Delta V_{corrected}$, represented the normalized and corrected output signals for the DNA hybridization of magnetically labeled ssDNA targets to the capture probes. Figure 6A2 demonstrated the detection of ALU115 and ALU247, the average of $\Delta V_{corrected}$ for each interaction, with a mean value based on at least eight GMR biosensors considered.

DNA methylation, along with DNA mutations, is widely recognized as valuable information for cancer diagnosis and prognosis. In a study conducted by Rizzi et al., a GMR-based bioassay method was presented that enables simultaneous profiling of DNA mutation and methylation events at specific sites.[67] Figure 6B depicts an innovative approach for DNA mutation and methylation analysis, involving the amplification of genomic DNA (for mutation analysis) or bisulfite-treated DNA (for methylation analysis) using nondiscriminatory primers. The resulting amplicons are then hybridized onto the surface of GMR biosensors, followed by precise melting curve measurements. The effectiveness of this method was demonstrated by its application to profile five mutation sites and four methylation sites in human melanoma cell lines. The approach accurately identified all mutation and methylation events and provided a quantitative assessment of methylation density, which was further validated through bisulfite pyrosequencing. These significant findings highlight the potential of utilizing temperature melting on a GMR biosensor as a semiquantitative technique for simultaneous profiling of DNA mutation and methylation. This innovative method holds great promise for advancing molecular diagnostic applications, particularly in cancer research and personalized medicine.

Later, in 2019, the same team combined methylation specific PCR (MSP) with melting curve analysis on GMR biosensors, greatly enhancing the methylation detection sensitivity.[97] Their findings successfully detected methylated CpG (5′-C-phosphate-G-3′) sites in the promoter regions of retinoic acid receptor β (RARβ) and the receptor tyrosine kinase KIT

https://doi.org/10.1021/acsabm.3c00592
ACS Appl. Bio Mater. 2023, 6, 4042−4059

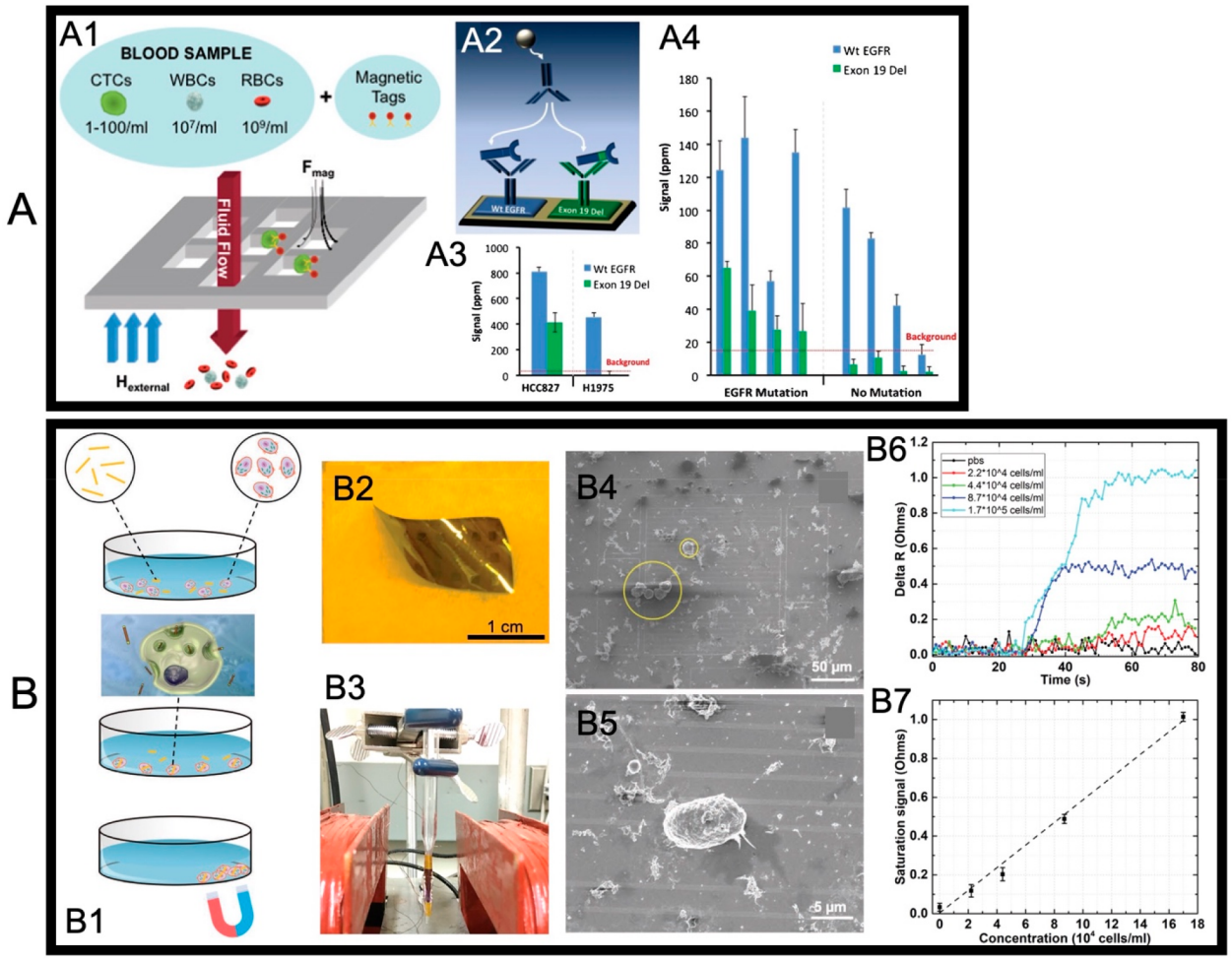

Figure 7. (A) GMR combined with magnetic separation for CTC scanning. (A1) Schematic of the magnetic sifter device. (A2) Detection of mutated and wild-type EGFR with GMR biosensors. Schematic showing anti-wild-type-EGFR (Wt EGFR) and anti-Exon 19 Del-EGFR (Exon 19 Del) functionalized on individual GMR biosensors. (A3) Results from cell lines with (HCC827) and without (H1975) Exon 19 Del captured from whole blood samples with the magnetic sifter, subjected to cell lysis and analyzed by the GMR biosensors. (A4) Assay results from eight patient samples, four with known Exon 19 Del mutations and four without Exon 19 Del mutations. The red dotted line represents the cutoff for the background signal. The error bars represent the standard deviation. (B) Flexible GMR biosensors for magnetically labeled OSCA-8 cell detection. (B1) Schematic illustration of the preparation process of magnetic nanowire labeled OCSA-8 cells. (B2) Photograph of one free-standing, flexible GMR biosensing chip. (B3) Photograph of the experimental setup for lab-on-a-needle detection of OSCA-8 cells. (B4, B5) Scanning electron microscope (SEM) images of magnetic nanowire labeled OSCA-8 cells on the GMR biosensor surface. Cells are highlighted in yellow circles. (B6) Real-time GMR biosensor signal for detecting different concentrations of OSCA-8 cells. (B7) Calibration curve of the saturation signal at different cell concentrations. (A) Reproduced with permission from ref 107. Copyright 2014 The Royal Society of Chemistry. (B) From ref 57. CC BY 4.0.

(KIT), genes that exhibit hypermethylation in 20−70% and 25−40% of melanomas, respectively.[98−100] They prepared samples with varying concentrations of methylated RARβ by diluting bisulfite-converted EST164 DNA (^{M}RARβ) into bisulfite-converted EST094 DNA (^{uM}RARβ), resulting in mixtures containing 100, 10, 1, 0.1, and 0% ^{M}RARβ. GMR biosensors were surface functionalized with complementary ssDNA capture probes for the methylated (M probe) and unmethylated (uM probe) RARβ. The denatured MSP products from these dilutions were hybridized to the capture probes on the GMR biosensor surface. After magnetic labeling of biotinylated target amplicons, the DNA melting curve was obtained by gradually increasing the temperature from 20 to 85 °C. Figure 6C presents the melting curves for MSP reactions performed at an intermediate annealing temperature of 62 °C, representing samples with 100, 1, and 0% ^{M}RARβ. During melting, C−T mismatches between methylated and unmethylated sequences caused significant variations in the melting temperature (T_m) of the two types of capture probes functionalized on individual GMR biosensors. In a fully methylated sample (Figure 6C1)), the perfect complementarity of the MSP product with the methylated probe yielded a high T_m for the M probe. Conversely, multiple C−T mismatches between the methylated sample and the uM probe led to a reduced T_m. The ΔT_m value signifies the difference in melting temperature between the two probes. A positive ΔT_m, as observed in Figure 6C1, indicates a higher proportion of methylated DNA in the sample. In a pure unmethylated sample (Figure 6C3), the melting curves of the M and uM probes are inverted, indicating the absence of methylation. In the case of a mixture containing 1% ^{M}RARβ (see Figure 6C2), the difference between the two curves decreased. Furthermore, by utilizing GMR melt curve analysis alone, they achieved multiplexed detection of methylated RARβ and KIT promoter regions down to 10% in the presence of their respective unmethylated genes. Additionally, by

https://doi.org/10.1021/acsabm.3c00592
ACS Appl. Bio Mater. 2023, 6, 4042−4059

incorporating MSP into this platform, they could detect even lower ratios of methylated DNA, making this technology a promising addition to the repertoire of techniques for assessing the methylation status of ctDNA in cancer screening and early detection.

3.3. GMR Biosensors for Tumor Cell Detection. The routine capture and analysis of circulating tumor cells (CTCs) from the blood of cancer patients holds immense potential in revolutionizing solid tumor oncology.[101−103] This advancement would introduce noninvasive "liquid biopsies", where blood samples containing CTCs replace the need for invasive tissue biopsies in the initial diagnosis and ongoing management of the disease. However, CTC enrichment and characterization present significant challenges, as these cells need to be captured from blood at extremely low levels.[104−106] Existing technologies for isolating CTCs suffer from limitations such as low throughput, inability to release captured cells, and reliance on costly instrumentation for enrichment and subsequent analysis. Magnetic biosensors designed to detect magnetically labeled target analytes offer a unique advantage. These labeled target analytes can be efficiently separated from biofluidic samples through a magnetic separation process, effectively enriching the target analytes during sample pretreatment. This enrichment step streamlines and facilitates the subsequent magnetic bioassay, making it more convenient and efficient. The combination of magnetic separation for sample enrichment and magnetic bioassay distinguishes magnetic biosensors from other types of label-based sensors, making them a standout choice for various diagnostic and analytical applications.

For instance, Earhart et al. conducted a study where they introduced a magnetic sifter, a microfluidic chip featuring an array of magnetic pores, to efficiently capture CTCs labeled with MNPs.[107] This device utilized an external magnetic field and sample pumping to induce strong magnetic forces on labeled cells, causing them to be attracted toward the pore edges, as shown in Figure 7A1. Unlabeled cells such as white blood cells (WBCs) and red blood cells (RBCs) passed through, while captured CTCs could be harvested. The magnetic sifter offers numerous advantages, including high capture efficiency, scalability, high throughput, a small capture area for rapid imaging, and the ability to harvest viable cells. The team employed this magnetic sifter to detect a specific mutated variant of the epidermal growth factor receptor (EGFR) in CTC lysates. After eluting the cells, they applied a membrane protein extraction protocol and introduced the lysate to GMR biosensors coated with antibodies targeting both wild-type (Wt EGFR) and mutated EGFR (Exon 19 Del), as schematically depicted in Figure 7A2. As shown in Figure 7A3, lysates from the lung tumor cell line HCC827 with the Exon 19 Del mutation caused a positive signal in the anti-Exon 19 Del-EGFR functionalized GMR biosensors, while the other lung tumor cell line (H1975) lacking the mutation showed no significant signal on GMR biosensors functionalized with anti-Exon 19 Del-EGFR antibodies. Both cell lines caused signals on GMR biosensors functionalized with anti-wild-type-EGFR antibodies since the wild-type capture and detection antibodies bind to epitopes on EGFR that are not mutated.

Furthermore, the researchers[107] tested blood samples from eight patients diagnosed with metastatic non-small cell lung cancer (NSCLC) with known mutational statuses. Following CTC enrichment using the magnetic sifter, they performed cell lysis and assessed the samples using GMR biosensors. As shown in Figure 7A4, among the four patients harboring the Exon 19 Del mutation, the presence of the mutant EGFR variant was positively detected, while the remaining four patients without the mutation did not yield a positive result. The study emphasizes the need for additional analysis and a larger sample size to establish confidence levels.

In 2023, Su et al. reported an ultraflexible GMR biosensor (Figure 7B2) for performing a lab-on-a-needle biopsy.[57] These ultraflexible GMR biosensing chips could be seamlessly integrated at the tip of medical tools without compromising their original functions. The flexible GMR biosensors exhibited impressive performance characteristics, including an MR ratio of 5.2% and a field sensitivity of 0.13%/Oe within the linear region. These values are comparable to those of their rigid GMR chip counterparts. Moreover, the flexible GMR biosensors demonstrated remarkable durability, maintaining their MR performance even after undergoing 500 cycles of compressive and tensile stress. This robustness makes them suitable for use on surfaces that are constantly in motion. To create the ultraflexible GMR biosensing chips, a standard nanofabrication process was employed, followed by a back-etching process to achieve a sub-20-μm thickness.[108] The resulting free-standing chips were then transferred onto flexible Kapton tape. Each individual flexible GMR chip consisted of 14 independently operating GMR biosensors, with each biosensor comprising 24 thin stripes measuring 150 μm × 0.75 μm. The entire chip occupied an area of approximately 3 cm^2. In Su et al.'s work,[57] flexible GMR biosensors were employed to detect canine osteosarcoma (OSCA-8) cells, showcasing their capability for accurate and sensitive cell detection. With a detection limit of 200 cells in a 20 μL sample, equivalent to a concentration of 10^4 cells/mL, these biosensors demonstrated their ability to perform real-time, sensitive, and quantitative cell detection. Uniform Ni magnetic nanowires measuring 1 μm in length were utilized to label the OSCA-8 cells. These nanowires were functionalized with polyethylene glycol (PEG) and then incubated with the cells in Dulbecco's modified Eagle's medium (DMEM) supplemented with 10% fetal bovine serum (FBS). Over a 48 h incubation period, the cells internalized the Ni magnetic nanowires. Subsequently, the cells were fixed using 2.5% glutaraldehyde and 0.1 M cacodylate. A magnetic separation step, depicted in Figure 7B1), was performed, and the cells were then resuspended in water for the GMR bioassay. Next, Ni magnetic nanowire labeled OSCA-8 cells were placed onto the surface of the GMR biosensor for further analysis. Upon complete evaporation of the water, the GMR biosensor surface revealed the presence of OSCA-8 cells labeled with magnetic nanowires (Figure 7B4,B5). To validate the platform's potential for practical applications, the flexible GMR chip was wrapped around the tip of a glass needle, enabling a bending radius of 1 mm (as depicted in Figure 7B3). Real-time monitoring of the magnetically labeled cells landing on the GMR biosensors was demonstrated. The resistance of the GMR biosensors was continuously measured under a constant applied field of 10 Oe, ensuring operation within the linear region of the MR response. Initially, a baseline was recorded for 20 s, followed by the addition of cell samples. The resulting change in resistance (ΔR) increased as the cell samples were introduced, reflecting the induced stray field from the magnetic nanowires. Eventually, ΔR reached saturation when the movement of the cells near the sensor surface reached

https://doi.org/10.1021/acsabm.3c00592
ACS Appl. Bio Mater. 2023, 6, 4042−4059

Table 1. Summary of Studies Employing GMR-Based Biosensors for Cancer/Tumor Detection

magnetic label	bioassay mechanism	target analyte	linear detection range	detection limit	tumor type	matrix	ref
128 nm MNP, 75 mg/mL	sandwich assay	AFP	1−1000 ng/mL	0.52 ng/mL	lung cancer, liver cancer, digestive tract cancer, prostatic cancer, etc.	buffer	63
		CEA	0.5−500 ng/mL	0.27 ng/mL			
		CYFRA21-1	0.5−100 ng/mL	0.25 ng/mL			
		NSE	1−200 ng/mL	0.5 ng/mL			
		SCC	0.5−70 ng/mL	0.3 ng/mL			
		PG I	2−200 ng/mL	1 ng/mL			
		PG II	1−100 ng/mL	0.5 ng/mL			
		CA19-9	4−800 U/mL	2 U/mL			
		total PSA	0.1−100 ng/mL	0.02 ng/mL			
		free PSA	0.1−50 ng/mL	0.07 ng/mL			
		free-β-hCG	0.5−200 ng/mL	0.3 ng/mL			
		Tg	5−2000 ng/mL	1 ng/mL			
Ademtech 200 nm bead	sandwich assay	CA125	1−128 U/mL[a]	3.7 U/mL	ovarian cancer	buffer	77
		HE4	2- 256 pg/mL[a]	7.4 pg/mL			
		IL6	2−256 pg/mL[a]	7.4 pg/mL			
Miltenyi Biotec, 130-048-101	indirect assay	PARK7	NA	NA	prostate cancer	serum	78
		TARDBP	NA	NA			
		TLN1	NA	NA			
		CALD1	NA	NA			
	sandwich assay	total PSA	NA	NA	prostate cancer	serum	78
		free PSA	NA	NA			
Dynabeads Myone streptavidin C1	sandwich assay	carcinoembryonic antigen	NA	10 pg/mL	colon cancer, lung cancer, ovarian cancer, gastric cancer, breast cancer, etc.	buffer	68
Micromod, 09-19-252	DNA hybridization assay	ALU115	NA	30 pM	NA	blood (cfDNA after purification)	60
		ALU247	NA	20 pM	NA		
Miltenyi Biotec, 130-048-101	DNA hybridization assay	three mutation sites in BRAF, two mutation sites in NRAS, two methylation sites in KIT promoter, and two methylation sites in RARβ promoter	NA	NA	melanoma cancer	cell culture medium (isolated genomic DNA after purification)	67
		methylated CpG sites in promoter regions of RARβ and receptor KIT	NA	0.1% methylated DNA			97
Miltenyi Biotec, 130-048-101	DNA hybridization assay	EGFR Exon 19 Del mutation	NA	0.01% mutant allelic fraction	NSCLC	blood (cfDNA after purification)	111
		substitution in exon 21 (L858R)	NA				
		T790M mutation	NA				
Miltenyi Biotec, 130-048-102	sandwich assay	EGFR Exon 19 Del mutation	NA	NA	NSCLC	blood (cfDNA after purification)	107
1-μm-long Ni magnetic nanowire	NA	OSCA-8 cells	(4.4−40) × 10^4 cells/mL	10^4 cells/mL	OSCA-8	buffer	57

[a]Estimated from data in the original paper.

https://doi.org/10.1021/acsabm.3c00592
ACS Appl. Bio Mater. 2023, 6, 4042−4059

Table 2. GMR-Based Biosensors for Cancer Screening

target analyte	tumor type	clinical sample size	comments	ref
AFP	lung cancer, liver cancer, digestive tract cancer, prostatic cancer, etc.	n = 58	good correlation coefficients (R^2 > 95%) when results compared with commercial immunosensors	63
CEA		n = 53		
CYFRA21-1		n = 39		
NSE		n = 32		
SCC		n = 56		
PG I		n = 27		
PG II		n = 29		
CA19-9		n = 44		
total PSA		n = 43		
free PSA		n = 38		
free-β-hCG		n = 36		
Tg		n = 24		
PARK7	prostate cancer	n = 99 (50 noncancer cases and 49 clinically localized prostate cancer cases)	statistically significant differences between prostate cancer and noncancer samples are observed, except for PARK7; p-values between noncancer and cancer cases: free/total PSA (p = 0.003), TARDBP (p < 0.001), TLN1 (p = 0.006) and CALD1 (p < 0.001), PARK (p = 0.771)	78
TARDBP				
TLN1				
CALD1				
free/total PSA ratio				
EGFR Exon 19 Del mutation	NSCLC	n = 36	87.5% sensitivity, 100% specificity	111
substitution in exon 21 (L858R)			90% sensitivity, 100% specificity	
T790M mutation			100% sensitivity, 96.3% specificity	

https://doi.org/10.1021/acsabm.3c00592
ACS Appl. Bio Mater. 2023, 6, 4042−4059

equilibrium (Figure 7B6). Furthermore, a linear relationship between the cell concentration and the saturated sensor signal was observed (Figure 7B7), confirming the flexible GMR biosensors' capability for quantitative and real-time cell detection.

3.4. GMR for Probing Magnetic Fluids Inside Tumors. Furthermore, GMR can be utilized for phantom imaging of magnetic fluids within tumors, in addition to detecting magnetically labeled biomarkers and cells. Gooneratne et al. conducted comprehensive theoretical and experimental studies using GMR biosensors to detect and estimate the weight density of MNPs inside agar phantoms and tumor tissues.[109,110] This approach was proposed to aid in magnetic hyperthermia therapy for tumors. Various factors influence the distribution of injected magnetic fluids in a tumor site, including particle size, surface characteristics, dosage, tumor and tissue heterogeneity, tumor size and pH, blood flow, and magnetic flux strength. However, it is important to recognize that the injected magnetic fluid can disperse into neighboring tissues, resulting in an uneven distribution and reduced fluid density within the tumor. To overcome this challenge, a minimally invasive GMR probe specifically designed for insertion near the tumor tissue has been developed. This probe allows for the analysis of magnetic fluid distribution within the tumor. By conducting this analysis, researchers can identify regions of inhomogeneity where the magnetic fluid is unevenly distributed in the tumor. In cases where such inhomogeneity is observed, techniques such as multisite injections can be employed to improve the homogeneity of magnetic fluid distribution within the tumor.

4. CONCLUSIVE REMARKS

GMR biosensors have a rich and successful history in the field of biosensing. Compared to other spintronic magnetic sensors such as anisotropic magnetoresistance (AMR) and magnetic tunnel junctions (MTJ), GMR biosensors have demonstrated superior maturity and robustness. In recent years, there have been significant advancements in utilizing GMR biosensors for cancer detection. Several studies have explored the application of GMR biosensors in detecting various cancer-related analytes. Notably, these works have been categorized based on the types of target analytes, as summarized in Table 1. The target analytes include protein biomarkers, ctDNA, and tumor cells. Studies exploring the use of GMR biosensors for cancer detection have yielded highly promising results. These biosensors have exhibited exceptional sensitivity and specificity in identifying cancer biomarkers, thereby enabling early and accurate diagnosis of cancer. The potential impact of GMR biosensors on cancer screening is significant, as they offer a noninvasive and cost-effective solution that could revolutionize current screening methods. Integrating GMR biosensors into large-scale cancer screening programs could prove transformative, given their scalability, rapid detection capabilities, and portability. The ability to detect cancer biomarkers quickly and reliably through GMR biosensors would enhance the effectiveness of cancer screening efforts, leading to earlier diagnoses and improved outcomes for patients. Moreover, the accessibility and ease of implementation of GMR biosensors in various clinical settings hold the promise of bringing cancer screening to more remote or resource-limited regions, making it a valuable tool in global cancer prevention and management strategies. As research and technology continue to advance, GMR biosensors hold the potential to play a crucial role in transforming cancer detection and screening practices, ultimately contributing to more proactive and effective cancer care.

One of the key advantages of GMR biosensors is their potential for low-cost production. The nano- and microfabrication technology behind GMR sensors is well-established, and these devices can be manufactured at a relatively low cost compared to other sensing technologies. This affordability opens avenues for their widespread adoption in healthcare settings, enabling cancer screening programs even in resource-limited areas. Moreover, GMR biosensors exhibit high sensitivity, allowing for the detection of minute concentrations of cancer-related analytes. This sensitivity enables early stage cancer detection, which is crucial for improving patient outcomes and reducing mortality rates. The high sensitivity of GMR biosensors also holds promise for monitoring treatment efficacy and disease progression, facilitating personalized cancer therapies.

It is important to acknowledge that the majority of GMR-based biosensors developed for cancer detection as well as reviewed in this work, encompassing protein biomarkers, ctDNA, and tumor cells, primarily focus on detecting samples with known analytes but unknown concentrations. Typically, these studies involve the detection of target analytes deliberately introduced into controlled environments, such as PBS, human serum, or human blood. These experiments serve as valuable proof-of-concept validations but remain distant from the ultimate goal of practical cancer screening. Regrettably, the literature contains only a limited number of research articles showcasing cancer screening conducted with clinical patient samples. To underscore the significance of these pioneering efforts toward real-world cancer screening, we have incorporated Table 2 to highlight the select studies that have ventured into the realm of cancer screening using actual clinical samples, shedding light on their contributions to advancing the field.

Looking toward the future, the development trajectory of GMR biosensors for cancer detection is focused on enhancing their sensitivity, specificity, and multiplexing capabilities. Nanofabrication techniques and biofunctionalization strategies are expected to play pivotal roles in optimizing GMR biosensor performance, enabling the simultaneous detection of an increasing number of cancer biomarkers. The integration of GMR biosensors with microfluidic systems and POCT platforms is anticipated to streamline the detection process, making it more accessible and convenient for healthcare settings. An exciting prospect lies in the combination of GMR biosensors with on-chip magnetic separation for analyte enrichment. This innovative approach could enable the detection of ultralow concentrations of tumor-specific biomarkers and CTCs from unprocessed blood samples. By pushing the limits of sensitivity, GMR biosensors hold the potential to revolutionize cancer detection, facilitating early intervention and improved patient outcomes.

As ongoing research and technological advancements continue to shape the field, GMR biosensors are poised to become key players in the future of cancer detection. Their ability to detect a wide range of cancer biomarkers simultaneously, with enhanced sensitivity and specificity, will significantly impact cancer diagnostics, guiding personalized treatment decisions and contributing to more effective cancer management strategies. With their potential for earlier and more accurate cancer detection, GMR biosensors hold the

https://doi.org/10.1021/acsabm.3c00592
ACS Appl. Bio Mater. 2023, 6, 4042−4059

promise of significantly improving patient prognosis and quality of life in the fight against cancer.

AUTHOR INFORMATION

Corresponding Author

Kai Wu − *Department of Electrical and Computer Engineering, Texas Tech University, Lubbock, Texas 79409, United States;* orcid.org/0000-0002-9444-6112; Email: kai.wu@ttu.edu

Authors

Shahriar Mostufa − *Department of Electrical and Computer Engineering, Texas Tech University, Lubbock, Texas 79409, United States;* orcid.org/0000-0002-3326-4817

Bahareh Rezaei − *Department of Electrical and Computer Engineering, Texas Tech University, Lubbock, Texas 79409, United States*

Parsa Yari − *Department of Electrical and Computer Engineering, Texas Tech University, Lubbock, Texas 79409, United States*

Kanglin Xu − *Department of Computer Science, Texas Tech University, Lubbock, Texas 79409, United States;* orcid.org/0009-0001-6898-9017

Jenifer Gómez-Pastora − *Department of Chemical Engineering, Texas Tech University, Lubbock, Texas 79409, United States*

Jiajia Sun − *State Key Laboratory of Electrical Insulation and Power Equipment, Xi'an Jiaotong University, Xi'an, Shaanxi Province 710049, China*

Zongqian Shi − *State Key Laboratory of Electrical Insulation and Power Equipment, Xi'an Jiaotong University, Xi'an, Shaanxi Province 710049, China;* orcid.org/0000-0003-3347-2058

Complete contact information is available at: https://pubs.acs.org/10.1021/acsabm.3c00592

Notes

The authors declare no competing financial interest.

ACKNOWLEDGMENTS

This study was financially supported by the Texas Tech University through the HEF New Faculty Startup, NRUF Start Up and Core Research Support Fund. B.R. acknowledges the Distinguished Graduate Student Assistantships (DGSA) offered by Texas Tech University.

REFERENCES

(1) Morris, M. C. *Fluorescence-Based Biosensors: From Concepts to Applications*; Academic Press: 2012; 416 pp.

(2) Girigoswami, K.; Akhtar, N. Nanobiosensors and Fluorescence Based Biosensors: An Overview. *International Journal of Nano Dimension* **2019**, *10* (1), 1−17.

(3) Weng, X.; Gaur, G.; Neethirajan, S. Rapid Detection of Food Allergens by Microfluidics ELISA-Based Optical Sensor. *Biosensors* **2016**, *6* (2), 24.

(4) Wu, L.; Li, G.; Xu, X.; Zhu, L.; Huang, R.; Chen, X. Application of Nano-ELISA in Food Analysis: Recent Advances and Challenges. *TrAC Trends in Analytical Chemistry* **2019**, *113*, 140−156.

(5) Hai, X.; Li, Y.; Zhu, C.; Song, W.; Cao, J.; Bi, S. DNA-Based Label-Free Electrochemical Biosensors: From Principles to Applications. *TrAC Trends in Analytical Chemistry* **2020**, *133*, 116098.

(6) Wu, Y.; Ali, S.; White, R. J. Electrocatalytic Mechanism for Improving Sensitivity and Specificity of Electrochemical Nucleic Acid-Based Sensors with Covalent Redox Tags—Part I. *ACS sensors* **2020**, *5* (12), 3833−3841.

(7) Vidic, J.; Manzano, M. Electrochemical Biosensors for Rapid Pathogen Detection. *Current Opinion in Electrochemistry* **2021**, *29*, 100750.

(8) Nabaei, V.; Chandrawati, R.; Heidari, H. Magnetic Biosensors: Modelling and Simulation. *Biosens. Bioelectron.* **2018**, *103*, 69−86.

(9) Wu, K.; Su, D.; Liu, J.; Saha, R.; Wang, J.-P. Magnetic Nanoparticles in Nanomedicine: A Review of Recent Advances. *Nanotechnology* **2019**, *30* (50), 502003.

(10) Yari, P.; Farmani, H.; Farmani, A. Steering of Guided Light with Graphene Metasurface for Refractive Index Sensing with High Figure of Merits. *Plasmonics* **2022**, *17* (1), 305−314.

(11) Mostufa, S.; Paul, A. K.; Chakrabarti, K. Detection of Hemoglobin in Blood and Urine Glucose Level Samples Using a Graphene-Coated SPR Based Biosensor. *OSA Continuum* **2021**, *4* (8), 2164−2176.

(12) Wang, Q.; Ren, Z.-H.; Zhao, W.-M.; Wang, L.; Yan, X.; Zhu, A.; Qiu, F.; Zhang, K.-K. Research Advances on Surface Plasmon Resonance Biosensors. *Nanoscale* **2022**, *14* (3), 564−591.

(13) Akgönüllü, S.; Özgür, E.; Denizli, A. Recent Advances in Quartz Crystal Microbalance Biosensors Based on the Molecular Imprinting Technique for Disease-Related Biomarkers. *Chemosensors* **2022**, *10* (3), 106.

(14) Maldonado, J.; Estévez, M.-C.; Fernández-Gavela, A.; González-López, J. J.; González-Guerrero, A. B.; Lechuga, L. M. Label-Free Detection of Nosocomial Bacteria Using a Nanophotonic Interferometric Biosensor. *Analyst* **2020**, *145* (2), 497−506.

(15) Dean, K. M.; Palmer, A. E. Advances in Fluorescence Labeling Strategies for Dynamic Cellular Imaging. *Nat. Chem. Biol.* **2014**, *10* (7), 512−523.

(16) Smith, A. M.; Duan, H.; Mohs, A. M.; Nie, S. Bioconjugated Quantum Dots for in Vivo Molecular and Cellular Imaging. *Advanced drug delivery reviews* **2008**, *60* (11), 1226−1240.

(17) Bhunia, S. K.; Saha, A.; Maity, A. R.; Ray, S. C.; Jana, N. R. Carbon Nanoparticle-Based Fluorescent Bioimaging Probes. *Sci. Rep.* **2013**, *3* (1), 1473.

(18) Hill, A. H.; Fu, D. Cellular Imaging Using Stimulated Raman Scattering Microscopy. *Analytical chemistry* **2019**, *91* (15), 9333−9342.

(19) Ramanavicius, S.; Ramanavicius, A. Charge Transfer and Biocompatibility Aspects in Conducting Polymer-Based Enzymatic Biosensors and Biofuel Cells. *Nanomaterials* **2021**, *11* (2), 371.

(20) Cavalcante, F. T.; de A. Falcão, I. R.; da S. Souza, J. E.; Rocha, T. G.; de Sousa, I. G.; Cavalcante, A. L.; de Oliveira, A. L.; de Sousa, M. C.; dos Santos, J. C. Designing of Nanomaterials-Based Enzymatic Biosensors: Synthesis, Properties, and Applications. *Electrochem* **2021**, *2* (1), 149−184.

(21) Ahangari, H.; Kurbanoglu, S.; Ehsani, A.; Uslu, B. Latest Trends for Biogenic Amines Detection in Foods: Enzymatic Biosensors and Nanozymes Applications. *Trends in Food Science & Technology* **2021**, *112*, 75−87.

(22) Wang, L.; Lin, J. Recent Advances on Magnetic Nanobead Based Biosensors: From Separation to Detection. *TrAC Trends in Analytical Chemistry* **2020**, *128*, 115915.

(23) Kim, S.-E.; Tieu, M. V.; Hwang, S. Y.; Lee, M.-H. Magnetic Particles: Their Applications from Sample Preparations to Biosensing Platforms. *Micromachines* **2020**, *11* (3), 302.

(24) Krishna, V. D.; Wu, K.; Su, D.; Cheeran, M. C.; Wang, J.-P.; Perez, A. Nanotechnology: Review of Concepts and Potential Application of Sensing Platforms in Food Safety. *Food microbiology* **2018**, *75*, 47−54.

(25) Wu, K.; Su, D.; Saha, R.; Liu, J.; Chugh, V. K.; Wang, J.-P. Magnetic Particle Spectroscopy: A Short Review of Applications Using Magnetic Nanoparticles. *ACS Applied Nano Materials* **2020**, *3* (6), 4972−4989.

(26) Wu, K.; Saha, R.; Su, D.; Krishna, V. D.; Liu, J.; Cheeran, M. C.-J.; Wang, J.-P. Magnetic-Nanosensor-Based Virus and Pathogen

Detection Strategies before and during COVID-19. *ACS Applied Nano Materials* **2020**, *3* (10), 9560−9580.
(27) Gloag, L.; Mehdipour, M.; Chen, D.; Tilley, R. D.; Gooding, J. J. Advances in the Application of Magnetic Nanoparticles for Sensing. *Adv. Mater.* **2019**, *31* (48), 1904385.
(28) He, J.; Huang, M.; Wang, D.; Zhang, Z.; Li, G. Magnetic Separation Techniques in Sample Preparation for Biological Analysis: A Review. *J. Pharm. Biomed. Anal.* **2014**, *101*, 84−101.
(29) Reokrungruang, P.; Chatnuntawech, I.; Dharakul, T.; Bamrungsap, S. A Simple Paper-Based Surface Enhanced Raman Scattering (SERS) Platform and Magnetic Separation for Cancer Screening. *Sens. Actuators, B* **2019**, *285*, 462−469.
(30) Zheng, Q.; Han, C.; Li, H. Selective and Efficient Magnetic Separation of Pb2+ via Gold Nanoparticle-Based Visual Binding Enrichment. *Chem. Commun.* **2010**, *46* (39), 7337−7339.
(31) Gómez-Pastora, J.; Xue, X.; Karampelas, I. H.; Bringas, E.; Furlani, E. P.; Ortiz, I. Analysis of Separators for Magnetic Beads Recovery: From Large Systems to Multifunctional Microdevices. *Sep. Purif. Technol.* **2017**, *172*, 16−31.
(32) Gómez-Pastora, J.; Karampelas, I. H.; Xue, X.; Bringas, E.; Furlani, E. P.; Ortiz, I. Magnetic Bead Separation from Flowing Blood in a Two-Phase Continuous-Flow Magnetophoretic Microdevice: Theoretical Analysis through Computational Fluid Dynamics Simulation. *J. Phys. Chem. C* **2017**, *121* (13), 7466−7477.
(33) Su, D.; Wu, K.; Saha, R.; Peng, C.; Wang, J.-P. Advances in Magnetoresistive Biosensors. *Micromachines* **2020**, *11* (1), 34.
(34) Wu, K.; Tonini, D.; Liang, S.; Saha, R.; Chugh, V. K.; Wang, J.-P. Giant Magnetoresistance Biosensors in Biomedical Applications. *ACS Appl. Mater. Interfaces* **2022**, *14* (8), 9945−9969.
(35) Wang, S. X.; Li, G. Advances in Giant Magnetoresistance Biosensors with Magnetic Nanoparticle Tags: Review and Outlook. *IEEE Trans. Magn.* **2008**, *44* (7), 1687−1702.
(36) Bailey, J.; Long, N.; Hunze, A. Eddy Current Testing with Giant Magnetoresistance (GMR) Sensors and a Pipe-Encircling Excitation for Evaluation of Corrosion under Insulation. *Sensors* **2017**, *17* (10), 2229.
(37) Borole, U. P.; Subramaniam, S.; Kulkarni, I. R.; Saravanan, P.; Barshilia, H. C.; Chowdhury, P. Highly Sensitive Giant Magnetoresistance (GMR) Based Ultra Low Differential Pressure Sensor. *Sensors and actuators A: Physical* **2018**, *280*, 125−131.
(38) Musuroi, C.; Oproiu, M.; Volmer, M.; Firastrau, I. High Sensitivity Differential Giant Magnetoresistance (GMR) Based Sensor for Non-Contacting DC/AC Current Measurement. *Sensors* **2020**, *20* (1), 323.
(39) Reig, C.; Cubells-Beltrán, M.-D.; Ramirez Muñoz, D. Magnetic Field Sensors Based on Giant Magnetoresistance (GMR) Technology: Applications in Electrical Current Sensing. *Sensors* **2009**, *9* (10), 7919−7942.
(40) Ha, M.; Cañón Bermúdez, G. S.; Kosub, T.; Mönch, I.; Zabila, Y.; Oliveros Mata, E. S.; Illing, R.; Wang, Y.; Fassbender, J.; Makarov, D. Printable and Stretchable Giant Magnetoresistive Sensors for Highly Compliant and Skin-Conformal Electronics. *Adv. Mater.* **2021**, *33* (12), 2005521.
(41) Kikitsu, A.; Higashi, Y.; Kurosaki, Y.; Shirotori, S.; Nagatsuka, T.; Suzuki, K.; Terui, Y. Magnetic Field Microscope Using High-Sensitivity Giant Magneto-Resistance Sensor with AC Field Modulation. *Jpn. J. Appl. Phys.* **2023**, *62* (SB), No. SB1007.
(42) Liang, S.; Sutham, P.; Wu, K.; Mallikarjunan, K.; Wang, J.-P. Giant Magnetoresistance Biosensors for Food Safety Applications. *Sensors* **2022**, *22* (15), 5663.
(43) Parikh, N. D.; Tayob, N.; Singal, A. G. Blood-Based Biomarkers for Hepatocellular Carcinoma Screening: Approaching the End of the Ultrasound Era? *Journal of hepatology* **2023**, *78* (1), 207−216.
(44) Fahrmann, J. F.; Marsh, T.; Irajizad, E.; Patel, N.; Murage, E.; Vykoukal, J.; Dennison, J. B.; Do, K.-A.; Ostrin, E.; Spitz, M. R.; et al. Blood-Based Biomarker Panel for Personalized Lung Cancer Risk Assessment. *Journal of Clinical Oncology* **2022**, *40* (8), 876−883.
(45) Chu, L.-Y.; Peng, Y.-H.; Weng, X.-F.; Xie, J.-J.; Xu, Y.-W. Blood-Based Biomarkers for Early Detection of Esophageal Squamous Cell Carcinoma. *World journal of gastroenterology* **2020**, *26* (15), 1708.
(46) Baibich, M. N.; Broto, J. M.; Fert, A.; Van Dau, F. N.; Petroff, F.; Etienne, P.; Creuzet, G.; Friederich, A.; Chazelas, J. Giant Magnetoresistance of (001) Fe/(001) Cr Magnetic Superlattices. *Physical review letters* **1988**, *61* (21), 2472.
(47) Binasch, G.; Grünberg, P.; Saurenbach, F.; Zinn, W. Enhanced Magnetoresistance in Layered Magnetic Structures with Antiferromagnetic Interlayer Exchange. *Phys. Rev. B* **1989**, *39* (7), 4828−4830.
(48) Cullity, B. D.; Graham, C. D. *Introduction to Magnetic Materials*; John Wiley & Sons: 2011.
(49) Wu, K.; Su, D.; Saha, R.; Wang, J.-P. Giant Magnetoresistance (GMR) Materials and Devices for Biomedical and Industrial Applications. *Spintronics: Materials, Devices and Applications* **2022**, 3−49.
(50) Bae, S. E.; Egelhoff, W. F., Jr.; Chen, P. J.; Zurn, S.; Sheppard, L.; Torok, E. J.; Judy, J. H. Application of α-Fe203 Bottom GMR Spin-Valve for Magnetoresistive Random Access Memory (MRAM). Presented at the International Conference on Ferrites, 2016.
(51) Apalkov, D.; Dieny, B.; Slaughter, J. M. Magnetoresistive Random Access Memory. *Proceedings of the IEEE* **2016**, *104* (10), 1796−1830.
(52) Ikegawa, S.; Mancoff, F. B.; Janesky, J.; Aggarwal, S. Magnetoresistive Random Access Memory: Present and Future. *IEEE Trans. Electron Devices* **2020**, *67* (4), 1407−1419.
(53) Gaster, R. S.; Xu, L.; Han, S.-J.; Wilson, R. J.; Hall, D. A.; Osterfeld, S. J.; Yu, H.; Wang, S. X. Quantification of Protein Interactions and Solution Transport Using High-Density GMR Sensor Arrays. *Nature Nanotechnol.* **2011**, *6* (5), 314−320.
(54) Klein, T.; Wang, Y.; Tu, L.; Yu, L.; Feng, Y.; Wang, W.; Wang, J.-P. Comparative Analysis of Several GMR Strip Sensor Configurations for Biological Applications. *Sensors and Actuators A: Physical* **2014**, *216*, 349−354.
(55) Feng, Y.; Liu, J.; Klein, T.; Wu, K.; Wang, J.-P. Localized Detection of Reversal Nucleation Generated by High Moment Magnetic Nanoparticles Using a Large-Area Magnetic Sensor. *J. Appl. Phys.* **2017**, *122* (12), 123901.
(56) Su, D.; Wu, K.; Wang, J.-P. Large-Area GMR Bio-Sensors Based on Reverse Nucleation Switching Mechanism. *J. Magn. Magn. Mater.* **2019**, *473*, 484−489.
(57) Su, D.; Wu, K.; Srinivasan, K.; Nemati, Z.; Zamani, R.; Chugh, V.; Saha, R.; Franklin, R.; Modiano, J.; Stadler, B.; et al. Ultra-Flexible Giant Magnetoresistance Biosensors for Lab-on-a-Needle Biosensing. *Advanced Materials Interfaces* **2023**, *10* (7), 2201417.
(58) Glathe, S.; Hübner, U.; Mattheis, R.; Seidel, P. Influence of Transverse Fields on Domain Wall Pinning in Ferromagnetic Nanostripes. *J. Appl. Phys.* **2012**, *112* (2), No. 023911.
(59) Melzer, M.; Karnaushenko, D.; Lin, G.; Baunack, S.; Makarov, D.; Schmidt, O. G. Direct Transfer of Magnetic Sensor Devices to Elastomeric Supports for Stretchable Electronics. *Adv. Mater.* **2015**, *27* (8), 1333−1338.
(60) Dias, T. M.; Cardoso, F. A.; Martins, S. A. M.; Martins, V. C.; Cardoso, S.; Gaspar, J. F.; Monteiro, G.; Freitas, P. P. Implementing a Strategy for On-Chip Detection of Cell-Free DNA Fragments Using GMR Sensors: A Translational Application in Cancer Diagnostics Using ALU Elements. *Anal. Methods* **2016**, *8* (1), 119−128.
(61) Wang, W.; Wang, Y.; Tu, L.; Klein, T.; Feng, Y. L.; Wang, J. P. Surface Modification for Protein and DNA Immobilization onto GMR Biosensor. *IEEE Trans. Magn.* **2013**, *49* (1), 296−299.
(62) Kim, D.; Marchetti, F.; Chen, Z.; Zaric, S.; Wilson, R. J.; Hall, D. A.; Gaster, R. S.; Lee, J.-R.; Wang, J.; Osterfeld, S. J.; et al. Nanosensor Dosimetry of Mouse Blood Proteins after Exposure to Ionizing Radiation. *Sci. Rep.* **2013**, *3* (1), 2234.
(63) Gao, Y.; Huo, W.; Zhang, L.; Lian, J.; Tao, W.; Song, C.; Tang, J.; Shi, S.; Gao, Y. Multiplex Measurement of Twelve Tumor Markers Using a GMR Multi-Biomarker Immunoassay Biosensor. *Biosens. Bioelectron.* **2019**, *123*, 204−210.

https://doi.org/10.1021/acsabm.3c00592
ACS Appl. Bio Mater. 2023, 6, 4042−4059

(64) Wang, W.; Wang, Y.; Tu, L.; Feng, Y.; Klein, T.; Wang, J.-P. Magnetoresistive Performance and Comparison of Supermagnetic Nanoparticles on Giant Magnetoresistive Sensor-Based Detection System. *Sci. Rep.* **2014**, *4*, 5716.
(65) Wu, K.; Klein, T.; Krishna, V. D.; Su, D.; Perez, A. M.; Wang, J.-P. Portable GMR Handheld Platform for the Detection of Influenza A Virus. *ACS Sensors* **2017**, *2*, 1594−1601.
(66) Su, D.; Wu, K.; Krishna, V.; Klein, T.; Liu, J.; Feng, Y.; Perez, A. M.; Cheeran, M. C.; Wang, J.-P. Detection of Influenza a Virus in Swine Nasal Swab Samples With a Wash-Free Magnetic Bioassay and a Handheld Giant Magnetoresistance Sensing System. *Frontiers in Microbiology* **2019**, *10*, 1077.
(67) Rizzi, G.; Lee, J. R.; Dahl, C.; Guldberg, P.; Dufva, M.; Wang, S. X.; Hansen, M. F. Simultaneous Profiling of DNA Mutation and Methylation by Melting Analysis Using Magnetoresistive Biosensor Array. *ACS Nano* **2017**, *11* (9), 8864−8870.
(68) Sun, X.; Lei, C.; Guo, L.; Zhou, Y. Giant Magneto-Resistance Based Immunoassay for the Tumor Marker Carcinoembryonic Antigen. *Microchimica Acta* **2016**, *183* (3), 1107−1114.
(69) Krishna, V. D.; Wu, K.; Perez, A. M.; Wang, J. P. Giant Magnetoresistance-Based Biosensor for Detection of Influenza A Virus. *Front. Microbiol.* **2016**, *7*, 400.
(70) Osterfeld, S. J.; Yu, H.; Gaster, R. S.; Caramuta, S.; Xu, L.; Han, S.-J.; Hall, D. A.; Wilson, R. J.; Sun, S.; White, R. L.; et al. Multiplex Protein Assays Based on Real-Time Magnetic Nanotag Sensing. *Proc. Natl. Acad. Sci. U. S. A.* **2008**, *105* (52), 20637−20640.
(71) Tsai, M.-Z.; Hsiung, C.-T.; Chen, Y.; Huang, C.-S.; Hsu, H.-Y.; Hsieh, P.-Y. Real-Time CRP Detection from Whole Blood Using Micropost-Embedded Microfluidic Chip Incorporated with Label-Free Biosensor. *Analyst* **2018**, *143* (2), 503−510.
(72) Lee, J.-R.; Choi, J.; Shultz, T. O.; Wang, S. X. Small Molecule Detection in Saliva Facilitates Portable Tests of Marijuana Abuse. *Analytical chemistry* **2016**, *88* (15), 7457−7461.
(73) Barderas, R.; Babel, I.; Diaz-Uriarte, R.; Moreno, V.; Suarez, A.; Bonilla, F.; Villar-Vazquez, R.; Capella, G.; Casal, J. I. An Optimized Predictor Panel for Colorectal Cancer Diagnosis Based on the Combination of Tumor-Associated Antigens Obtained from Protein and Phage Microarrays. *Journal of proteomics* **2012**, *75* (15), 4647−4655.
(74) Barrett, C. L.; DeBoever, C.; Jepsen, K.; Saenz, C. C.; Carson, D. A.; Frazer, K. A. Systematic Transcriptome Analysis Reveals Tumor-Specific Isoforms for Ovarian Cancer Diagnosis and Therapy. *Proc. Natl. Acad. Sci. U. S. A.* **2015**, *112* (23), E3050−E3057.
(75) Zhong, L.; Coe, S. P.; Stromberg, A. J.; Khattar, N. H.; Jett, J. R.; Hirschowitz, E. A. Profiling Tumor-Associated Antibodies for Early Detection of Non-Small Cell Lung Cancer. *Journal of Thoracic Oncology* **2006**, *1* (6), 513−519.
(76) Zhang, J.-Y. Tumor-Associated Antigen Arrays to Enhance Antibody Detection for Cancer Diagnosis. *Cancer detection and prevention* **2004**, *28* (2), 114−118.
(77) Klein, T.; Wang, W.; Yu, L.; Wu, K.; Boylan, K. L.; Vogel, R. I.; Skubitz, A. P.; Wang, J.-P. Development of a Multiplexed Giant Magnetoresistive Biosensor Array Prototype to Quantify Ovarian Cancer Biomarkers. *Biosens. Bioelectron.* **2019**, *126*, 301−307.
(78) Xu, L.; Lee, J.-R.; Hao, S.; Ling, X. B.; Brooks, J. D.; Wang, S. X.; Gambhir, S. S. Improved Detection of Prostate Cancer Using a Magneto-Nanosensor Assay for Serum Circulating Autoantibodies. *PloS one* **2019**, *14* (8), No. e0221051.
(79) Su, D.; Um, J.; Moreno, J.; Nemati, Z.; Srinivasan, K.; Chen, J.; Zamani Kouhpanji, M. R.; Shore, D.; Wu, K.; Kosel, J.; et al. GMR Biosensing with Magnetic Nanowires as Labels for the Detection of Osteosarcoma Cells. *Sensors and Actuators A: Physical* **2023**, *350*, 114115.
(80) Mathios, D.; Johansen, J. S.; Cristiano, S.; Medina, J. E.; Phallen, J.; Larsen, K. R.; Bruhm, D. C.; Niknafs, N.; Ferreira, L.; Adleff, V.; et al. Detection and Characterization of Lung Cancer Using Cell-Free DNA Fragmentomes. *Nat. Commun.* **2021**, *12* (1), 5060.
(81) Corcoran, R. B.; Chabner, B. A. Application of Cell-Free DNA Analysis to Cancer Treatment. *New England Journal of Medicine* **2018**, *379* (18), 1754−1765.
(82) Oxnard, G. R.; Klein, E. A.; Seiden, M. V.; Hubbell, E.; Venn, O.; Jamshidi, A.; Zhang, N.; Beausang, J. F.; Gross, S.; Kurtzman, K. N.; et al. Simultaneous Multi-Cancer Detection and Tissue of Origin (TOO) Localization Using Targeted Bisulfite Sequencing of Plasma Cell-Free DNA (CfDNA). *Annals of Oncology* **2019**, *30*, v912.
(83) Siejka-Zielińska, P.; Cheng, J.; Jackson, F.; Liu, Y.; Soonawalla, Z.; Reddy, S.; Silva, M.; Puta, L.; McCain, M. V.; Culver, E. L.; et al. Cell-Free DNA TAPS Provides Multimodal Information for Early Cancer Detection. *Sci. Adv.* **2021**, *7* (36), No. eabh0534.
(84) Xu, J.; Wu, W.; Wu, C.; Mao, Y.; Qi, X.; Guo, L.; Lu, R.; Xie, S.; Lou, J.; Zhang, Y.; et al. A Large-Scale, Multicentered Trial Evaluating the Sensitivity and Specificity of Digital PCR versus ARMS-PCR for Detecting CtDNA-Based EGFR p. T790M in Non-Small-Cell Lung Cancer Patients. *Translational Lung Cancer Research* **2021**, *10* (10), 3888.
(85) Feng, Q.; Gai, F.; Sang, Y.; Zhang, J.; Wang, P.; Wang, Y.; Liu, B.; Lin, D.; Yu, Y.; Fang, J. A Comparison of QuantStudio™ 3D Digital PCR and ARMS-PCR for Measuring Plasma EGFR T790M Mutations of NSCLC Patients. *Cancer Management and Research* **2018**, *10*, 115−121.
(86) Madic, J.; Piperno-Neumann, S.; Servois, V.; Rampanou, A.; Milder, M.; Trouiller, B.; Gentien, D.; Saada, S.; Assayag, F.; Thuleau, A.; et al. Pyrophosphorolysis-Activated Polymerization Detects Circulating Tumor DNA in Metastatic Uveal Melanoma. *Clin. Cancer Res.* **2012**, *18* (14), 3934−3941.
(87) Shi, J.; Liu, Q.; Sommer, S. S. Detection of Ultrarare Somatic Mutation in the Human TP53 Gene by Bidirectional Pyrophosphorolysis-activated Polymerization Allele-specific Amplification. *Human mutation* **2007**, *28* (2), 131−136.
(88) Garcia, J.; Forestier, J.; Dusserre, E.; Wozny, A.-S.; Geiguer, F.; Merle, P.; Tissot, C.; Ferraro-Peyret, C.; Jones, F. S.; Edelstein, D. L.; et al. Cross-Platform Comparison for the Detection of RAS Mutations in CfDNA (DdPCR Biorad Detection Assay, BEAMing Assay, and NGS Strategy). *Oncotarget* **2018**, *9* (30), 21122.
(89) van Ginkel, J. H.; Huibers, M. M.; van Es, R. J.; de Bree, R.; Willems, S. M. Droplet Digital PCR for Detection and Quantification of Circulating Tumor DNA in Plasma of Head and Neck Cancer Patients. *BMC Cancer* **2017**, *17* (1), 428.
(90) O'Leary, B.; Hrebien, S.; Beaney, M.; Fribbens, C.; Garcia-Murillas, I.; Jiang, J.; Li, Y.; Huang Bartlett, C.; Andre, F.; Loibl, S.; et al. Comparison of BEAMing and Droplet Digital PCR for Circulating Tumor DNA Analysis. *Clinical Chemistry* **2019**, *65* (11), 1405−1413.
(91) Al Zoughbi, W.; Fox, J.; Beg, S.; Papp, E.; Hissong, E.; Ohara, K.; Keefer, L.; Sigouros, M.; Kane, T.; Bockelman, D.; et al. Validation of a Circulating Tumor DNA-Based next-Generation Sequencing Assay in a Cohort of Patients with Solid Tumors: A Proposed Solution for Decentralized Plasma Testing. *oncologist* **2021**, *26* (11), e1971−e1981.
(92) Clark, T. A.; Chung, J. H.; Kennedy, M.; Hughes, J. D.; Chennagiri, N.; Lieber, D. S.; Fendler, B.; Young, L.; Zhao, M.; Coyne, M.; et al. Analytical Validation of a Hybrid Capture−Based next-Generation Sequencing Clinical Assay for Genomic Profiling of Cell-Free Circulating Tumor DNA. *Journal of Molecular Diagnostics* **2018**, *20* (5), 686−702.
(93) Marchetti, A.; Palma, J. F.; Felicioni, L.; De Pas, T. M.; Chiari, R.; Del Grammastro, M.; Filice, G.; Ludovini, V.; Brandes, A.; Chella, A.; et al. Early Prediction of Response to Tyrosine Kinase Inhibitors by Quantification of EGFR Mutations in Plasma of NSCLC Patients. *Journal of Thoracic Oncology* **2015**, *10* (10), 1437−1443.
(94) Zhu, G.; Ye, X.; Dong, Z.; Lu, Y. C.; Sun, Y.; Liu, Y.; McCormack, R.; Gu, Y.; Liu, X. Highly Sensitive Droplet Digital PCR Method for Detection of EGFR-Activating Mutations in Plasma Cell−Free DNA from Patients with Advanced Non−Small Cell Lung Cancer. *Journal of Molecular Diagnostics* **2015**, *17* (3), 265−272.

https://doi.org/10.1021/acsabm.3c00592
ACS Appl. Bio Mater. 2023, 6, 4042−4059

(95) Chabon, J. J.; Hamilton, E. G.; Kurtz, D. M.; Esfahani, M. S.; Moding, E. J.; Stehr, H.; Schroers-Martin, J.; Nabet, B. Y.; Chen, B.; Chaudhuri, A. A.; et al. Integrating Genomic Features for Non-Invasive Early Lung Cancer Detection. *Nature* **2020**, *580* (7802), 245−251.
(96) Umetani, N.; Kim, J.; Hiramatsu, S.; Reber, H. A.; Hines, O. J.; Bilchik, A. J.; Hoon, D. S. Increased Integrity of Free Circulating DNA in Sera of Patients with Colorectal or Periampullary Cancer: Direct Quantitative PCR for ALU Repeats. *Clinical chemistry* **2006**, *52* (6), 1062−1069.
(97) Nesvet, J.; Rizzi, G.; Wang, S. X. Highly Sensitive Detection of DNA Hypermethylation in Melanoma Cancer Cells. *Biosens. Bioelectron.* **2019**, *124*, 136−142.
(98) Dahl, C.; Abildgaard, C.; Riber-Hansen, R.; Steiniche, T.; Lade-Keller, J.; Guldberg, P. KIT Is a Frequent Target for Epigenetic Silencing in Cutaneous Melanoma. *Journal of Investigative Dermatology* **2015**, *135* (2), 516−524.
(99) Dahl, C.; Christensen, C.; Jönsson, G.; Lorentzen, A.; Skjodt, M. L.; Borg, Å.; Pawelec, G.; Guldberg, P. Mutual Exclusivity Analysis of Genetic and Epigenetic Drivers in Melanoma Identifies a Link Between P14ARF and RARβ Signaling. *Molecular Cancer Research* **2013**, *11* (10), 1166−1178.
(100) Dahl, C.; Guldberg, P. E. R. The Genome and Epigenome of Malignant Melanoma. *Apmis* **2007**, *115* (10), 1161−1176.
(101) Shen, Z.; Wu, A.; Chen, X. Current Detection Technologies for Circulating Tumor Cells. *Chem. Soc. Rev.* **2017**, *46* (8), 2038−2056.
(102) Paterlini-Brechot, P.; Benali, N. L. Circulating Tumor Cells (CTC) Detection: Clinical Impact and Future Directions. *Cancer letters* **2007**, *253* (2), 180−204.
(103) Hong, B.; Zu, Y. Detecting Circulating Tumor Cells: Current Challenges and New Trends. *Theranostics* **2013**, *3* (6), 377.
(104) Gabriel, M. T.; Calleja, L. R.; Chalopin, A.; Ory, B.; Heymann, D. Circulating Tumor Cells: A Review of Non−EpCAM-Based Approaches for Cell Enrichment and Isolation. *Clinical chemistry* **2016**, *62* (4), 571−581.
(105) Arya, S. K.; Lim, B.; Rahman, A. R. A. Enrichment, Detection and Clinical Significance of Circulating Tumor Cells. *Lab Chip* **2013**, *13* (11), 1995−2027.
(106) Song, Y.; Tian, T.; Shi, Y.; Liu, W.; Zou, Y.; Khajvand, T.; Wang, S.; Zhu, Z.; Yang, C. Enrichment and Single-Cell Analysis of Circulating Tumor Cells. *Chemical science* **2017**, *8* (3), 1736−1751.
(107) Earhart, C. M.; Hughes, C. E.; Gaster, R. S.; Ooi, C. C.; Wilson, R. J.; Zhou, L. Y.; Humke, E. W.; Xu, L.; Wong, D. J.; Willingham, S. B.; et al. Isolation and Mutational Analysis of Circulating Tumor Cells from Lung Cancer Patients with Magnetic Sifters and Biochips. *Lab Chip* **2014**, *14* (1), 78−88.
(108) Chen, J. Y.; Lau, Y. C.; Coey, J. M. D.; Li, M.; Wang, J. P. High Performance MgO-Barrier Magnetic Tunnel Junctions for Flexible and Wearable Spintronic Applications. *Sci. Rep* **2017**, *7*, 7.
(109) Gooneratne, C. P.; Iwahara, M.; Yamada, S.; Kakikawa, M. GMR Sensor Application in Detecting and Estimating Magnetic Fluid Weight Density inside Various Size Tumors. *Journal of the Magnetics Society of Japan* **2009**, *33* (3), 175−178.
(110) Gooneratne, C. P.; Kurnicki, A.; Yamada, S.; Mukhopadhyay, S. C.; Kosel, J. Analysis of the Distribution of Magnetic Fluid inside Tumors by a Giant Magnetoresistance Probe. *PLoS One* **2013**, *8* (11), No. e81227.
(111) Nesvet, J. C.; Antilla, K. A.; Pancirer, D. S.; Lozano, A. X.; Preiss, J. S.; Ma, W.; Fu, A.; Park, S.-M.; Gambhir, S. S.; Fan, A. C.; et al. Giant Magnetoresistive Nanosensor Analysis of Circulating Tumor DNA Epidermal Growth Factor Receptor Mutations for Diagnosis and Therapy Response Monitoring. *Clinical chemistry* **2021**, *67* (3), 534−542.

https://doi.org/10.1021/acsabm.3c00592
ACS Appl. Bio Mater. 2023, 6, 4042−4059